

FEFFLAP: A Finite Element Program for Analysis of Fluid-Driven Fracture Propagation in Jointed Rock

Vol. 1: Theory and Programmer's Manual

A. R. Ingraffea

R. J. Shaffer

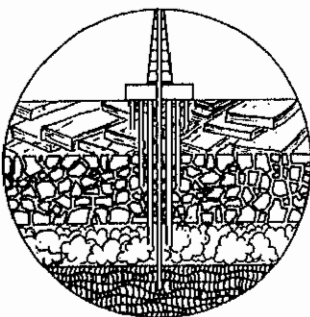
F. E. Heuze

**Prepared for
Morgantown Energy Technology Center
Morgantown, WV**

March, 1985

**Lawrence
Livermore
National
Laboratory**

This is an informal report intended primarily for internal or limited external distribution. The opinions and conclusions stated are those of the author and may or may not be those of the Laboratory.



Unconventional Gas Program

Western Gas Sands Research

DISCLAIMER

This document was prepared as an account of work sponsored by an agency of the United States Government. Neither the United States Government nor the University of California nor any of their employees, makes any warranty, express or implied, or assumes any legal liability or responsibility for the accuracy, completeness, or usefulness of any information, apparatus, product, or process disclosed, or represents that its use would not infringe privately owned rights. Reference herein to any specific commercial products, process, or service by trade name, trademark, manufacturer, or otherwise, does not necessarily constitute or imply its endorsement, recommendation, or favoring by the United States Government or the University of California. The views and opinions of authors expressed herein do not necessarily state or reflect those of the United States Government or the University of California, and shall not be used for advertising or product endorsement purposes.

Printed in the United States of America
Available from
National Technical Information Service
U.S. Department of Commerce
5285 Port Royal Road
Springfield, VA 22161
Price: Printed Copy \$; Microfiche \$4.50

<u>Page Range</u>	<u>Domestic Price</u>	<u>Page Range</u>	<u>Domestic Price</u>
001-025	\$ 7.00	326-350	\$ 26.50
026-050	8.50	351-375	28.00
051-075	10.00	376-400	29.50
076-100	11.50	401-426	31.00
101-125	13.00	427-450	32.50
126-150	14.50	451-475	34.00
151-175	16.00	476-500	35.50
176-200	17.50	501-525	37.00
201-225	19.00	526-550	38.50
226-250	20.50	551-575	40.00
251-275	22.00	576-600	41.50
276-300	23.50	601-up ¹	
301-325	25.00		

¹Add 1.50 for each additional 25 page increment, or portion thereof from 601 pages up.

INDEX

	Page
1. GENERAL DESCRIPTION OF FEFFLAP.....	1
1.1 Introduction.....	1
1.2 Preprocessing.....	2
1.3 Structural Analysis.....	3
1.3.1 Element Library.....	3
1.3.2 Boundary Conditions.....	3
1.3.3 Multiple Load Capability.....	3
1.3.4 Stiffness Assembly.....	7
1.3.5 Equation Solver.....	7
1.4 Coupling of Flow and Structural Analyses.....	7
1.5 Post Processing.....	7
2. SOLID MECHANICS.....	9
2.1 Solids.....	9
2.2 Joints.....	9
3. FRACTURE MECHANICS.....	11
3.1 Historical Perspective.....	11
3.2 Discrete Crack Models for Geomaterials.....	15
3.2.1 The Linear Model.....	16
3.2.1.1 Stress intensity factor computation.....	16
3.2.1.2 Mixed-mode interaction formulas.....	23
3.2.1.3 Predicting crack increment length.....	30
3.2.2 The Nonlinear Model.....	33
3.2.2.1 The process zone.....	33
3.2.2.2 Stress versus COD models.....	35
3.2.2.3 A nonlinear crack propagation algorithm.....	39
4. FLUID MECHANICS.....	43
4.1 Fluid Flow Model.....	43
4.2 Minimum Aperture for Fluid Flow.....	44

INDEX

	Page
5. PROGRAM STRUCTURE.....	45
5.1 Code Routines.....	45
5.1.1 Control.....	45
5.1.2 Input/Output Operations.....	45
5.1.3 Structural and Flow Analyses.....	50
5.1.4 Graphics Operations.....	50
5.2 Memory Management.....	53
6. REFERENCES.....	61
7. ACKNOWLEDGMENTS.....	64

1. GENERAL DESCRIPTION OF FEFFLAP

1.1 Introduction

FEFFLAP (Finite Element Fracture and Flow Analysis Program) is a finite element program for two-dimensional analysis of static or quasi-static propagation of discrete fractures in homogeneous or jointed media. The fractures, or cracks, can be driven by a variety of loading conditions, including internal fluid pressure. The code contains quite sophisticated fracture mechanics: stress intensity factors are calculated with special crack tip finite elements; fracture instability and angle of propagation are estimated from any one of three fracture criteria; induced cracks can change direction and can interact with pre-existing fractures. FEFFLAP also provides for non-linear behavior of discontinuities such as geologic interfaces and joints, and for steady-state viscous fluid flow in the cracks and the discontinuities.

FEFFLAP has evolved from three building blocks:

- . the FEFAP (Finite Element Fracture Analysis Program) for discrete fracture propagation in rock and concrete [1-3].
- . the JTFLO code for coupled analysis of flow in fractured media [4], as further enhanced at LLNL.
- . the JPLAXD code for static analysis of structures in jointed rock [5].

The program is both incremental and iterative. Incremental means the ability to apply loads in a stepwise fashion. This emulates to some degree the time dependency of a loading, such as a borehole being pressurized in rock; however, the solution at each load increment is steady state, not transient. Iterative means that the calculations are done repeatedly within each load increment to satisfy the non-linear constitutive relations of geological materials, and the coupling between the flow and the structural stress changes.

FEFFLAP can calculate the exact load required to initiate or extend any crack. A multiple load capability is available in the code, for complicated fracturing problems involving simultaneously loads that can change and loads

that do not change. An example of such a problem is hydraulic fracturing of a gas field from a borehole: the field stresses at infinity are constant in time during fracture propagation, and the fluid pressure in the borehole is variable; note, however, that the field (in-situ) stresses can vary arbitrarily in space, inside the domain. FEFFLAP also has the standard set of permissible boundary conditions (loads, displacements, pressures).

The operation of the code depends heavily on graphics because it is a fully interactive model. The user can alter crack propagation by changing conditions during the analysis, can iterate on fluid flow and joint nonlinearities, as required for convergence, and can change aspect ratios of elements at each increment of crack propagation, to improve accuracy. The code can accommodate up to 10 different materials and can propagate up to 9 cracks at a time; these numbers can be increased with minimal modifications.

This report describes the theory underlying the code. The logic of the program is also given in some details to enable potential users to make modifications and additions, as well as to facilitate transfer of the current version, developed on a CRAY, to other machines. General characteristics of the program are further explained in the rest of this chapter. The version of the code described in this report is labeled FEFFLAP 1.0.

1.2 Preprocessing

An input file must be generated for each problem. Currently this is done by constructing the file from a teletype. Automatic node generation via the input file is possible with ordered quadrilateral elements. Care is not required in the order of node numbering because a mesh optimizer (bandwidth minimizer) is used. The flow network is simply overlaid on the elastic grid so that a flow node exists at the end of each joint element. Flow nodes are numbered according to increasing joint element number. The exact form of the input file is given in a companion document.*

*R. J. Shaffer, A. R. Ingraffea, and F. E. Heuze, "FEFFLAP: A Computer Program for Analysis of Fluid-Driven Fracture Propagation in Jointed Rock - Vol. 2: User's Manual", Lawrence Livermore National Laboratory, UCID-20369, 1985.

1.3 Structural Analysis

1.3.1 Element Library

The element library consists of seven elements of three types: solid, joint and flow elements. The flow element is the simplest; it is a line element with two nodes. The remaining six elements are shown in Figure 1. The joint (interface) element has six nodes and a prescribed thickness. The five solid elements range from a truss element with three nodes to the quadrilateral with eight nodes. The singular elements, Figure 1 e) and f), are described in detail later, in the fracture mechanics section. Singular elements are used only at crack tips and are designed to respond to the square root singularity in the stresses, for the calculation of stress intensity factors.

1.3.2 Boundary Conditions

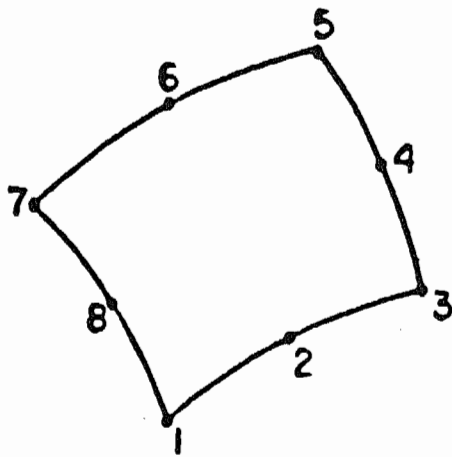
The structural part of FEFFLAP accepts three types of loading conditions:

- . point loads
- . edge loads
- . initial nodal displacements.

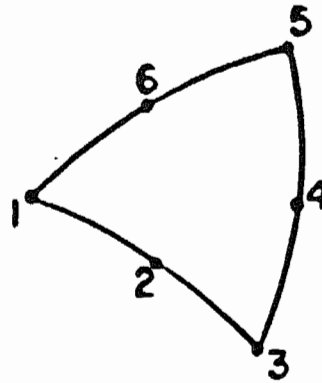
In addition, the fluid flow part of FEFFLAP uses two types of boundary conditions: pressure and flow rate. These are prescribed at the flow nodes.

1.3.3 Multiple Load Capability

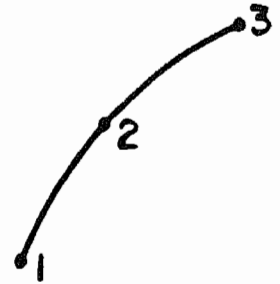
Analysis of fracturing processes involves the determination of the stress magnitude required to cause fracture initiation at a point or fracture instability at a crack tip. When a single load set is used it is trivial to find the necessary load to cause fracture initiation or instability; the load is simply proportioned up or down according to material strength or fracture toughness. Typical physical processes usually involve more than one type of loading. An example is an underground hydraulically induced fracture. When multiple load sets are used, the determination of the appropriate stress level is quite complicated. These complications can be clarified with the aid of Figure 2.



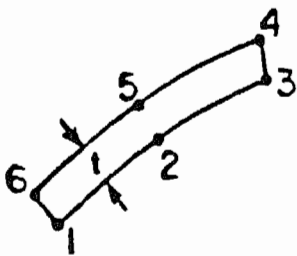
a) Quadrilateral (Q8)



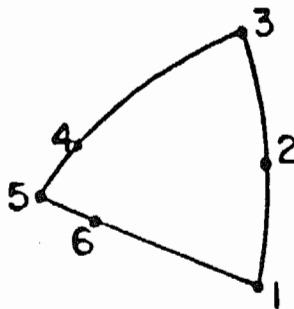
b) Triangle (LST)



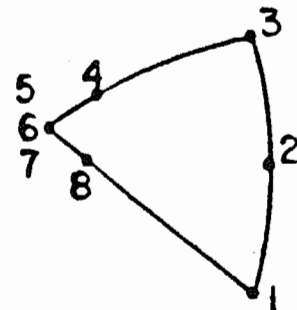
c) Truss



d) Interface



e) Singular LST



f) Singular (collapsed) Q8

Figure 1: FEFLLAP Element Library

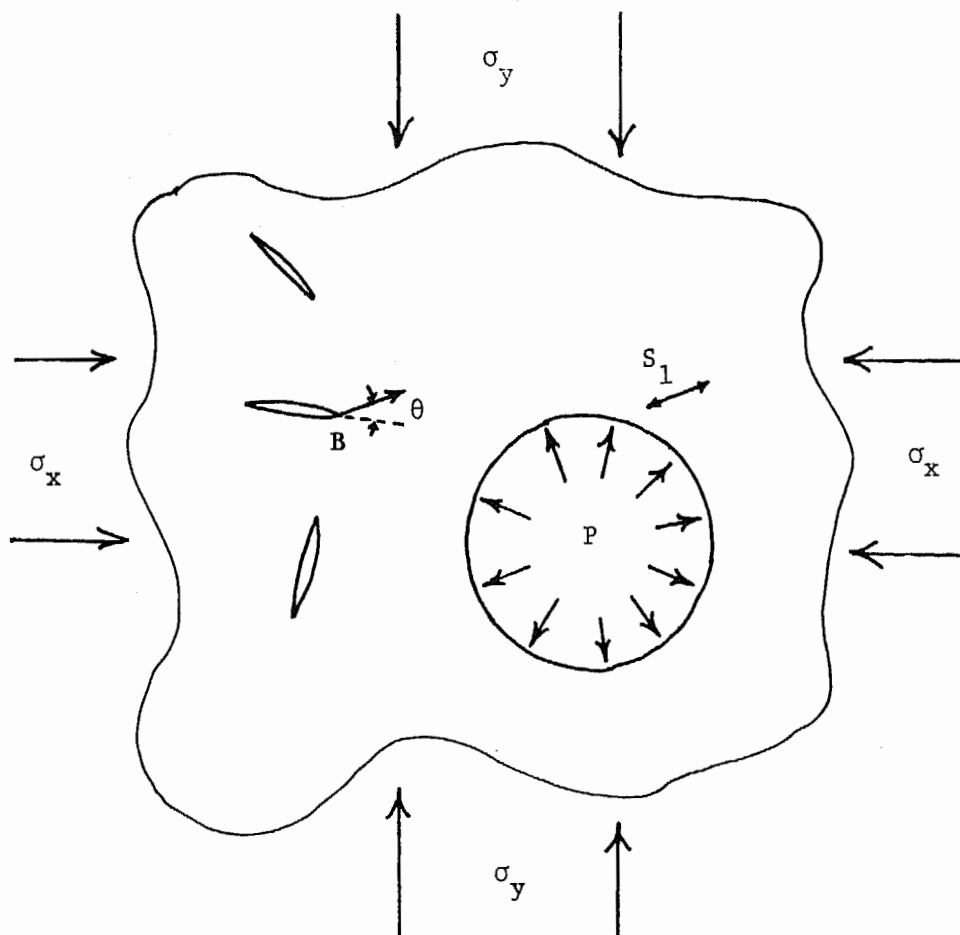


Figure 2: An Example of a Multiple Load Problem

The field stresses at infinity σ_x and σ_y in Figure 2 are constant; note, however, that they can generate a non-uniform stress field inside the domain. The pressure in the borehole, P , has to be determined so that a crack will initiate, or an existing crack will propagate. Starting with an initial value of $P = P_0$, a stress analysis indicates that the maximum tensile principal stress, S_1 , is at the location and orientation shown in Figure 2. In addition, crack tip B has the highest stress intensity factors and, according to an appropriate fracture criterion, would propagate at an angle θ . Since P_0 is insufficient to cause crack initiation (S_1 is less than the tensile

strength of the material) or crack propagation (the stress intensity factors are less than the critical stress intensity factors of the material) a new value, P_1 , must be obtained. This can be calculated directly for crack tip B and for principal stress S_1 . The problem is that when P is increased to P_1 , stress redistribution can take place so that the new maximum principal stress is at a different location and/or at a different orientation. Similarly, crack tip B may want to propagate at a different angle and, possibly, a different crack tip may have larger stress intensity factors than crack tip B. Consequently, the determination of the correct value of P involves sequential calculations of P_1 followed by a search for the maximum principal stress or the maximum stress intensity factors. It is, therefore, an iterative process. The procedure for calculating P_1 for crack initiation is as follows: the maximum principal stress S_1 is at an angle ϕ with respect to the cartesian coordinate system. The stress S_1 can be constructed from the sum of the stresses due to each load set:

$$S_1 = \sigma'_{xv} + \sigma'_{xc} \quad (1)$$

where v and c denote variable and constant stress, respectively. The superscript (prime) refers to rotated stresses, i.e.:

$$\sigma'_x = \sigma_x \cos^2 \phi + 2\tau_{xy} \sin \phi \cos \phi + \sigma_y \sin^2 \phi. \quad (2)$$

Since one wants S_1 to be equal to T (the tensile strength) for crack initiation at angle ϕ one has

$$T = \kappa \sigma'_{xv} + \sigma'_{xc} \quad (3)$$

where κ is a multiplicative factor. Hence

$$\kappa = \frac{T - \sigma'_{xc}}{\sigma'_{xv}}. \quad (4)$$

The variable load vector is factored up by κ and a complete stress analysis is done to determine if the point of initiation has changed or if the angle ϕ has changed. If so, a new κ must be calculated and another stress analysis performed. This is done until the angle and point of initiation do not change.

Figure 2 represents a highly simplified example. In FEFFLAP the variable load is entirely general and includes, for example, pressure due to fluid flow in cracks and interfaces.

1.3.4 Stiffness Assembly

FEFFLAP is formulated in the displacement approach of the finite element method, and the structural stiffness matrix is prepared by direct assembly of elemental stiffnesses.

1.3.5 Equation Solver

The linear simultaneous equations in FEFFLAP are solved directly by a highly efficient skyline solver.

1.4 Coupling of Flow and Structural Analyses

FEFFLAP is constructed from solid elements that are linear and joint elements that can behave nonlinearly. It is coupled with a flow program that uses current structural displacements to obtain flow rates and pressure in cracks and joints. The mechanics of the solid-fluid flow interaction in FEFFLAP are as follows: the fluid pressures produce boundary conditions that are used to elastically determine the apertures of the joints and cracks. The apertures are then used in the fluid flow model to determine flow rates and pressures. This process is repeated until convergence occurs. The nonlinear behavior of joints is also iterated upon until convergence within the flow iteration loop. The logic of the flow/structure coupling is described in Figure 3.

1.5 Post Processing

Three types of output are provided to the user: monitor graphics, teletype output, and accumulated output that is put into a file named by the user. On the CRAY computer the monitor graphics can be accumulated into a graphics file if desired and hardcopy can then be obtained after execution of the program. In addition, FILE1 contains the values of all the variables after the last flow and joint iterations, or the last crack increment. Therefore, additional processing could be done if desired.

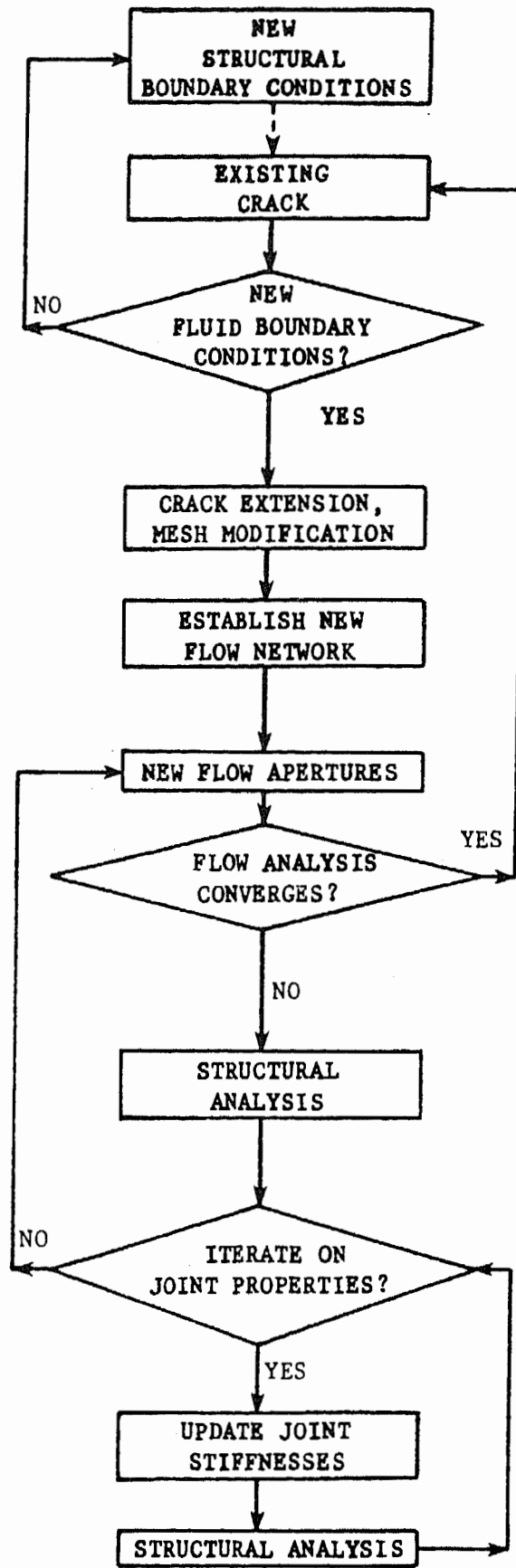


Figure 3: Logic of the Coupling Between Structural and Flow Analyses in FEFLAP

2. SOLID MECHANICS

The solids part of FEFFLAP is composed of linearly elastic finite elements as material models and nonlinear joint finite elements to represent preexisting cracks or interfaces between dissimilar materials.

2.1 Solids

Each solid material in FEFFLAP is characterized by the following:

- . Young's modulus
- . Poisson's ratio
- . fracture toughness
- . uniaxial compressive strength
- . uniaxial tensile strength
- . tensile strength in tensile-compressive region.

2.2 Joints

Joint elements are characterized by six parameters:

- . normal stiffness
- . shear stiffness
- . tensile strength
- . cohesion
- . friction angle
- . maximum closure.

Normal stiffness decreases by three orders of magnitude at each iteration when the normal tensile strength has been exceeded and the joint has opened. In addition, frictional stress is set to zero and the shear stiffness is given a very small value when the joint opens. Figure 4 provides the nomenclature for joints in direct shear and Figure 5 depicts how the shear stiffness (KS) changes when the peak shear stress is exceeded. Figure 6 shows how the normal stiffness is adjusted when joint closure occurs. Joint behavior is discussed more fully in [5]. Joints in FEFFLAP are non-dilatant in shear. The addition of dilation would require another level of iteration in the code [6].

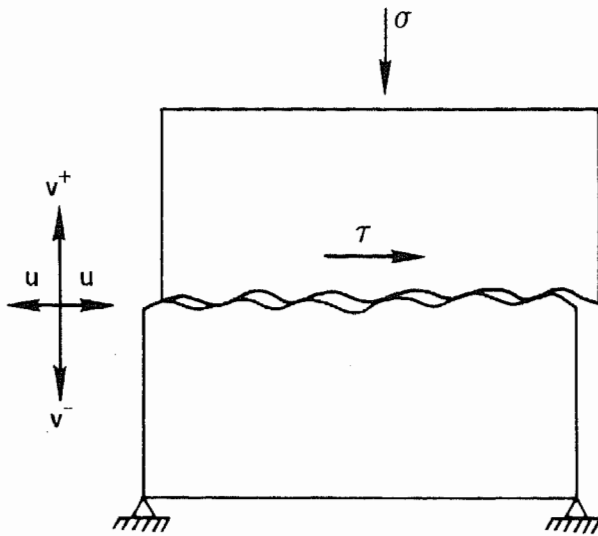


Figure 4: Nomenclature for Joints in Direct Shear

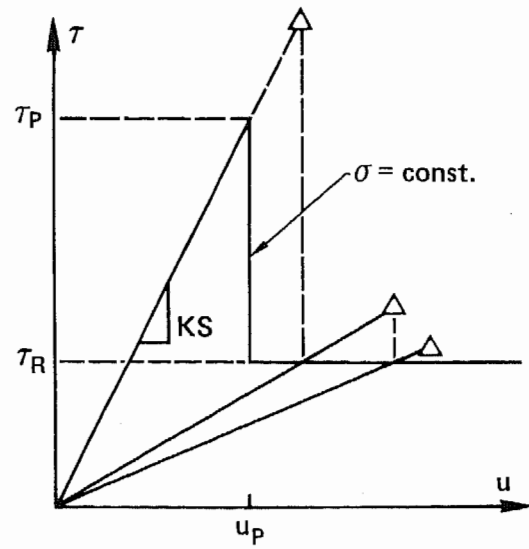


Figure 5: Strain-Softening of Joints in Direct Shear

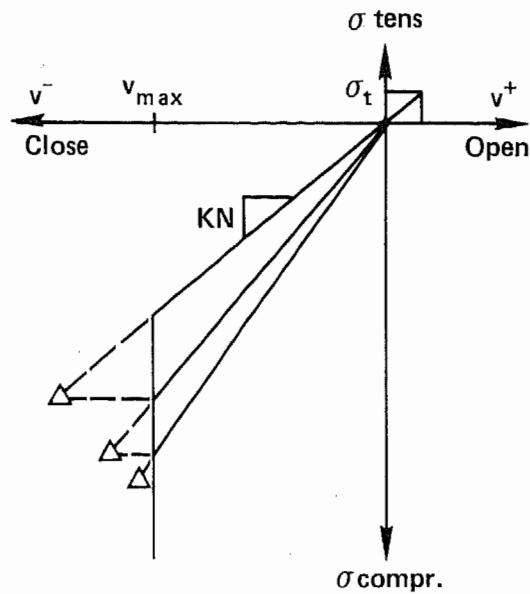


Figure 6: Joint Behavior in the Normal Direction

3. FRACTURE MECHANICS

3.1 Historical Perspective

The use of the finite element method to model cracking of structures can be completely characterized by two essential elements: the manner of inclusion of a crack in the finite element mesh, and the criterion for crack instability and direction of growth.

In the early efforts, notably in concrete and rock structures [7-9], cracks were modeled discretely. That is, a crack was formed by separation of previously common element edges. The resultant change in nodal connectivity was made at each stage of propagation. If the crack trajectory was assumed a priori, double-nodes could be provided along the element edges that would become the crack path [8]. Alternatively, all nodes could be doubled initially and only those close to a predicted path would be separated [10]. The early discrete crack approaches all suffered two major drawbacks:

- . lack of physical fidelity in that crack trajectory was constrained to follow predefined element boundaries.
- . increasing cost and decreasing efficiency in that additional degrees-of-freedom had to be added with each crack increment. This meant that the size of the analysis grew, as did the bandwidth of the structural stiffness matrix.

The "smeared crack" approach, introduced for concrete structures [11], overcame those drawbacks and quickly replaced the discrete approach.

In the early efforts, the criterion for instability and direction of growth, the second essential modeling element, did not derive from any fracture mechanics notion. Rather, a simple tensile strength approach was employed. When the principal tensile stress computed in the elements ahead of the discrete or smeared crack tip reached some measure of strength, those elements were "cracked". Direction of propagation was assumed to be normal to that of the principal stress.

Given this starting point, one must ask what has changed in the ensuing fifteen years of usage of the finite element method for crack propagation analysis of rock structures. In the authors' opinion, the answer is: not much. A smeared crack, tensile strength fracture model is the state-of-the-practice for research and production oriented codes. The capabilities for shear transfer across, and the intersecting of, cracks have been added. However, the smeared crack model has remained largely unaffected by ongoing developments in finite elements, equation solving, user-computer interaction, and fracture mechanics. It is essential to recognize that, in its formative years, the constant strain triangle, simple equation solvers, key-punching of data, batch analysis mode, and elementary constitutive models were the order of the day.

FEFFLAP uses crack modeling approaches which markedly depart from today's common practice. It integrates many of the innovations in the aforementioned areas. For crack propagation, these methods are characterized by:

- . a return to the discrete crack,
- . linear and nonlinear fracture mechanics
- . and a new essential modeling element: the use of interactive-adaptive computer graphics techniques as an integral part of the analysis process.

Before proceeding to the new models themselves, additional background material related to the evolution of these essential elements needs to be detailed.

It is not surprising that the initial usage of the discrete crack approach was short lived. To overcome the first of the drawbacks cited above, manual remeshing after each crack increment would have been required. It was well known that bandwidth minimization was essential to analysis efficiency, but, to overcome the second drawback, manual renumbering for minimal bandwidth of an increasingly complex mesh also would have been required. Clearly, given the mesh generation and bandwidth minimization capability of the middle 1960's, an adversary relationship existed between the discrete crack and the finite element method. It was the encumbrances of the above mentioned drawbacks, and not a new view of the physics of the problem, which led to the early and nearly ubiquitous adoption of the smeared crack approach. There have been arguments proposed that the smeared crack is more realistic; however, given the scale differences between the finite element width typically used in

analysis and usually predicated by other considerations [12] and the physical width of a crack and associated process zone as observed in experiments [13], these arguments are difficult to accept.

In trying to return to the more physically palatable discrete crack idea there have been sporadic efforts towards eliminating its drawbacks, such as the novel approach of Ngo [14]. However, if a discrete model were to become acceptable at any level of use, a method of automatic regeneration of the mesh to accommodate arbitrary and incrementally changing crack trajectories would have to be found. This method would properly introduce the displacement and traction variations across and along the crack, properly mesh around the crack tip, allow cracks to cross pre-existing discontinuities, and minimally increase the bandwidth of the structural stiffness matrix. Let us review the various advances over the last decade that have, in fact, led to the development of such a method.

First, take the capability for automatic mesh generation. Few would, today, consider complete manual generation of even a two-dimensional mesh. Automatic mesh generators of various degrees of sophistication are now in widespread use. At their highest level they make use of generalized lofting, splining, and other elegant topological manipulations to produce complex two and three-dimensional meshes from minimal user input [15-17]. But, in fact, the problem at hand is simpler in that discrete crack modeling requires only local modifications to an existing mesh. A solution to this problem for two-dimensional and axisymmetric meshes is implemented in FEFFLAP. The algorithm developed is based on the local remeshing requirements which result from:

- . a discrete crack crossing an element.
- . ascertaining which element is the next to be entered, when a crack emerges from an element side or a corner node.
- . checking if the crack will stop in the next element entered.

The algorithm has proven to be versatile and robust. Common pathological situations which may arise in remeshing are automatically diagnosed and corrected. Examples include:

- a crack about to cross joint and rock bolt elements: since the latter should not be broken by the crack, modifications such as those shown in Figure 7 are automatically performed.
- when a crack breaks an element in two, and if one of the new elements would have a large aspect ratio, then one of the sides of the original element will be shifted to coincide with the crack; consequently, the crack now propagates between two elements of acceptable aspect ratio.

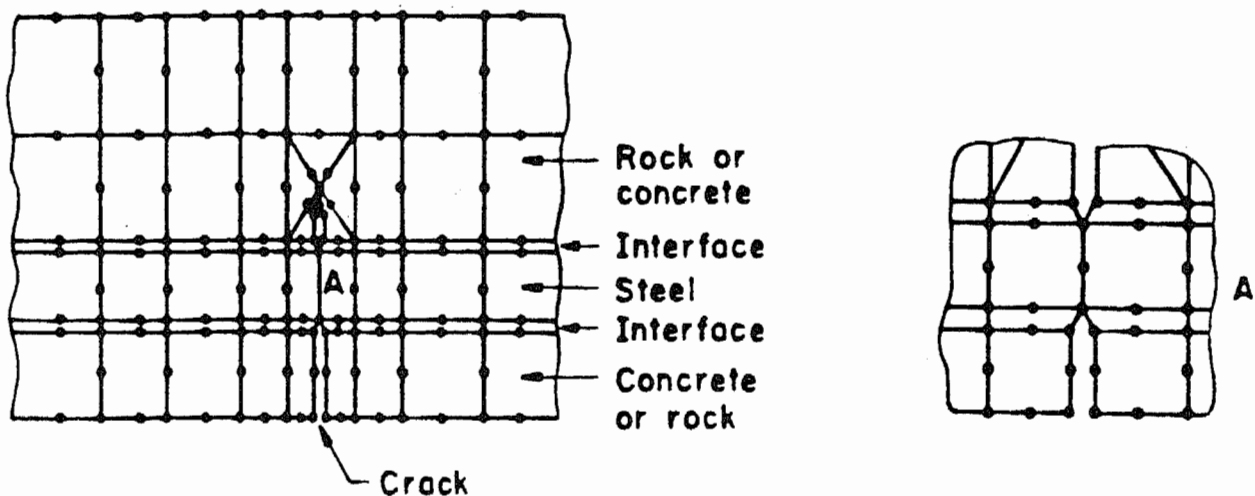


Figure 7. Example of Automatic Mesh Modification Performed by FEFFLAP:
a Crack Crosses a Reinforcing Bar or Rock Bolt.

To summarize, an algorithm has been developed which automatically remeshes in the vicinity of a crack to accommodate arbitrary trajectories. This eliminates the first drawback to the original discrete crack approach.

Next, is the bandwidth problem. Two potential solutions have arisen over the last decade: the frontal technique or automatic bandwidth minimizers. The latter approach [18] has been adopted for FEFFLAP. After each crack increment has created new nodes, all nodes are automatically renumbered to approach minimum bandwidth and all the data keyed to nodes numbers are relabeled. The entire process is transparent to the user and typically adds only a few percent additional CPU time. Consequently, the second drawback originally ascribed to the discrete crack approach has also been eliminated. It is true that the size of the problem still increases with crack propagation as compared to a smeared crack approach, but this is as it should be: the

deformation field of a structure becomes more complex with cracking, and mesh refinement is justified to maintain a reasonable level of accuracy in the analysis.

Finally, the most exciting development in computer analysis in the last fifteen years probably is the area of computer graphics. Interactive graphics has improved productivity and put the engineer back in control of his sophisticated analyses. Control of decision-making in analysis has undergone drastic change. Not much control needed to be exercised over the analysis process in the simple linear analyses of the mid-1960's; with the initial database specified there were no more judgment decisions left to be made by the analyst. However, with nonlinear analyses encouraged by the complex constitutive models of the 1970's, processing of the initial database often necessitated revisions such as load step size, error tolerances, mesh gradation, or solution algorithm itself. Interactive graphics are used in FEFFLAP to display in real time:

- . all stages of mesh development
- . "zoomed" details of meshes
- . deflected shapes
- . principal stress fields
- . crack trajectories
- . energy release rate curves
- . predicted crack increment directions
- . stress-intensity factor interaction diagrams, and most importantly
- . numerical information essential to the analysis decision making process.

The last item implies that FEFFLAP is not only interactive-graphic, but that it is also "interactive-adaptive". This term is used to describe methods, essential to nonlinear analysis, in which parameters, algorithms, meshes, and problem descriptions are selected or changed by the user during the analysis itself.

3.2 Discrete Crack Models for Geomaterials

Two types of fracture models have been implemented into the discrete cracking approach in FEFFLAP [3,19-21]. The first model is based on classical, linear

elastic fracture mechanics. Governing parameters are the stress-intensity factors and the fracture toughness. The latter quantity is still designated K_{Ic} , despite sparsity of information regarding the difference, if any, between plane strain and other fracture toughness measures in geomaterials. As usual the assumption is made that the process zone associated with the crack is much smaller than the crack length; again, information concerning thickness effects on process zone size is inconclusive to date. At the scale of the crack length, the material is thus assumed to act as a homogeneous solid.

Whereas the linear model assigns a critical stress intensity to the crack tip, the second, nonlinear model, assumes that stress intensity is always zero. This model is based on the assumption that a narrow process zone exists ahead of the traction free crack. The process zone itself is idealized as a discontinuity in displacement, but not in stress; in effect it is a "fictitious crack" [22-24]. The process zone constitutive law relates tractions, both normal and tangential, to crack-opening-displacement (COD).

These models are related by scale. The small crack-tip process zone in the linear model can be viewed as the nonlinear process zone at a much smaller scale. A very short crack would be described by the nonlinear model, a very long crack, with sufficient COD over most of its length, by the linear approach.

Details concerning formulation of these models and their manner of implementation into a discrete crack idealization are presented next.

3.2.1. The Linear Model

3.2.1.1 Stress intensity factor computations

In the linear model, stress intensity factors control crack stability and trajectory. The sequence of events in the implementation of this model into a two-dimensional mixed-mode crack propagation code is:

1. Compute stress intensity factors for present crack tip location and loading.
2. Substitute K_I and K_{II} into mixed-mode interaction formula. Compute new crack direction and assess stability. If crack is unstable, continue. If stable, go to step 4.

3. Remesh for a selected increment of propagation. Repeat steps 1 through 3 until crack is stable or fracture occurs.
4. If crack is stable, raise load level until instability is predicted by interaction formula. Continue with step 3.

The accurate prediction of load level, angle change, and length corresponding to each increment of crack propagation requires accurate computation of mixed-mode stress intensity factors. Efficiency is also desirable since many analyses may be required in a single problem.

The displacement correlation technique has been adopted for FEFFLAP. It is accurate and efficient. Displacements computed at nodes near the crack tip are correlated with the theoretical values. For example, in pure Mode I, near tip displacements relative to the crack tip are,

$$u = \frac{K_I}{4G} \sqrt{\frac{r}{2\pi}} \left[(2\kappa - 1) \cos \frac{\theta}{2} - \cos \frac{3\theta}{2} \right] + \dots \quad (5)$$

$$v = \frac{K_I}{4G} \sqrt{\frac{r}{2\pi}} \left[(2\kappa - 1) \sin \frac{\theta}{2} - \sin \frac{3\theta}{2} \right] + \dots$$

where,

- u = displacement parallel to crack axis
- v = displacement normal to crack axis
- ν = Poisson's ratio
- G = shear modulus
- κ = $(3-4\nu)$ for plane strain
- κ = $(3-\nu)/(1+\nu)$ for plane stress

Taking $\theta = 180^\circ$, and $r = r_{AB}$, in Figure 8, the K_I computed by the finite element method is expressed by,

$$K_I = \sqrt{\frac{2\pi}{r_{AB}}} \frac{2G}{(\kappa+1)} (v_B - v_A) \quad (6)$$

For pure Mode II and plane stress,

$$u = \frac{K_{II}}{4G} \sqrt{\frac{r}{2\pi}} \left[(2\kappa+3) \sin \frac{\theta}{2} + \sin \frac{3\theta}{2} \right] + \dots \quad (7)$$

$$v = \frac{-K_{II}}{4G} \sqrt{\frac{r}{2\pi}} \left[(2\kappa-3) \cos \frac{\theta}{2} + \cos \frac{3\theta}{2} \right] + \dots$$

And an expression for K_{II} is, for $\theta = 180^\circ$, $r = r_{AB}$,

$$K_{II} = \sqrt{\frac{2\pi}{r_{AB}}} \frac{2G}{(\kappa+1)} (u_B - u_A) \quad (8)$$

For mixed-mode loading, the near-tip displacements are given by linear combinations of Equation (5) and Equation (7). However, it can be seen that the combined expressions for u and v uncouple at $\theta = \pm 180^\circ$. Consequently, Equations (6) and (8) can be used for a crack on a symmetry or anti-symmetry line. In the general, asymmetrical case, the stress intensity factors must be computed from crack-opening and crack-sliding displacements, COD and CSD, respectively, where, for $r = r_{AB} = r_{AC}$,

$$\begin{aligned} \text{COD} &= v_B - v_C \\ \text{CSD} &= u_B - u_C \end{aligned} \quad (9)$$

Substituting Equations (5) and (7) into Equation (9), and solving for K_I and K_{II} yields,

$$K_I = \sqrt{\frac{2\pi}{r_{AB}}} \frac{G}{(\kappa+1)} (v_B - v_C) \quad (10)$$

$$K_{II} = \sqrt{\frac{2\pi}{r_{AB}}} \frac{G}{(\kappa+1)} (u_B - u_C)$$

Equations (10) are the most general form for computing stress intensity factors using the displacement correlation technique. The success of this

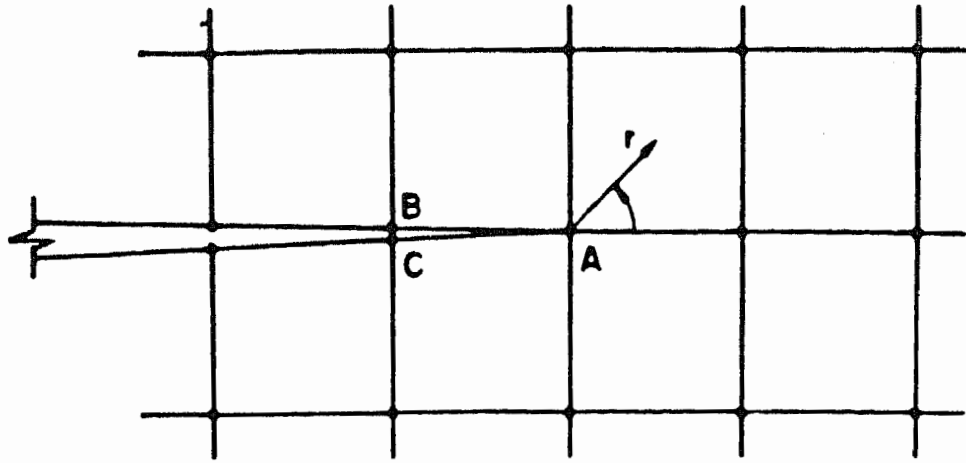


Figure 8. Crack Tip Region Nodal Lettering for Equation 6 Through 10.

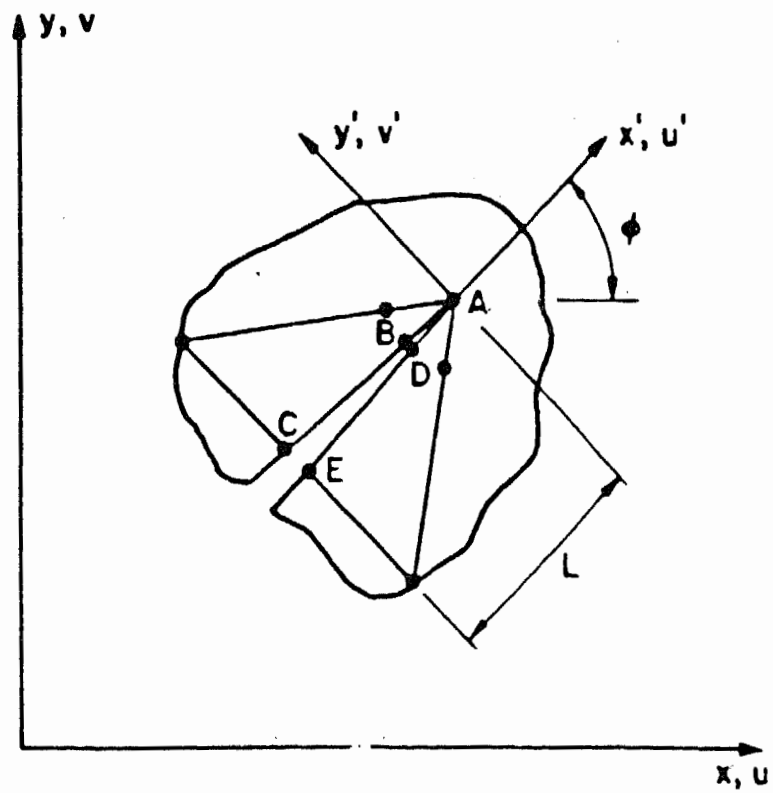


Figure 9. Crack Tip Region Nodal Lettering for Equation 11 and 12.

technique depends on an accurate modeling of the theoretical $r^{1/2}$ displacement variation near the crack tip. Many workers have applied a number of finite element method techniques to this end. Earliest efforts employed brute force. Constant strain triangles (CST) were used with extremely fine meshes near the crack tip. The major drawback to using CST's in fracture problems is the very large number of degrees of freedom required for engineering accuracy even for a single crack.

The next step in finite element developments for the displacement correlation technique was to take a hint from the elasticity solution for the crack tip displacements and create an element containing an $r^{1/2}$ interpolation function. In practice, this has been done by a number of workers using elements of various shapes. The most convenient of these, the quarter-point isoparametric triangle [25,26], is the singular element employed by the authors. Combination of this singular element with the extraction technique outlined below makes programming for stress intensity factor computation almost trivial compared to the efforts of less than a decade ago.

The application of the displacement correlation technique to quarter-point singular elements was first proposed by Shih et al. [27] for Mode I problems. The generalization to mixed-mode is straightforward [28] and goes as follows. First, let a crack tip be surrounded by quarter-point singular elements and the crack face nodes be lettered as shown in Figure 9. The only meshing constraint at this point is that the lengths of the two elements containing the lettered nodes be the same, i.e., $\overline{AC} = \overline{AE}$. Next, expand the lettered nodal displacements in terms of the element shape functions and with respect to the crack tip coordinate system shown in Figure 9. This leads to expressions of the following form:

$$\begin{aligned} v' &= v'_A + (-3v'_A + 4v'_B - v'_C) \sqrt{r/L} + (2v'_A - 4v'_B + 2v'_C)r/L \\ u' &= u'_A + (-3u'_A + 4u'_B - u'_C) \sqrt{r/L} + (2u'_A - 4u'_B + 2u'_C)r/L \end{aligned} \quad (11)$$

Similar expressions are obtained along the \overline{ADE} ray. Taking the difference between the expression along the two rays yields a computed crack opening or crack sliding profile.

Now the displacement expansions from the asymptotic analytical solution, Equation (5), are evaluated at $\theta = \pm 180^\circ$ to compute a theoretical crack opening or crack sliding profile. Equating like powers of r in the computed and theoretical profiles leads directly to:

$$K_I = \sqrt{\frac{2\pi}{L}} \frac{G}{\kappa+1} [4(v'_B - v'_D) + v'_E - v'_C] \quad (12)$$

$$K_{II} = \sqrt{\frac{2\pi}{L}} \frac{G}{\kappa+1} [4(u'_B - u'_D) + u'_E - u'_C]$$

in which,

- L = length of singularity element side along the ray,
- v' = crack-opening nodal displacements,
- u' = crack-sliding nodal displacements.

The primes indicate that the global coordinate nodal displacements have been transformed to the crack-tip coordinate system defined in Figure 9. The above procedure has also been generalized to the three-dimensional case [28].

In FEFPLAP, the displacements and coordinates of the crack face nodes belonging to the quarter-point elements are flagged and retrieved for each crack increment solution. The accuracy of the method will be discussed with reference to the meshes shown in Figure 10 for the ASTM standard three-point bend specimen.

The accuracy of Equations 12 depends on a number of mesh characteristics. For example, Figure 11 shows two- and three-dimensional finite element results compared to the ASTM solution, known to be accurate within 1 percent, with L/a as a parameter (L = length of side of singularity element along crack; a = crack length). The differences in the two-dimensional results vary from -8 percent at $L/a = 0.20$ to -1 percent at $L/a = 0.03$. The three-dimensional results bracket the ASTM value, and centerline values are within ± 5 percent difference over the entire L/a range tested. The conclusion here is that there is an optimum L/a ratio; however, it is problem and mesh dependent. Experience on a large number of two- and three-dimensional analyses has shown

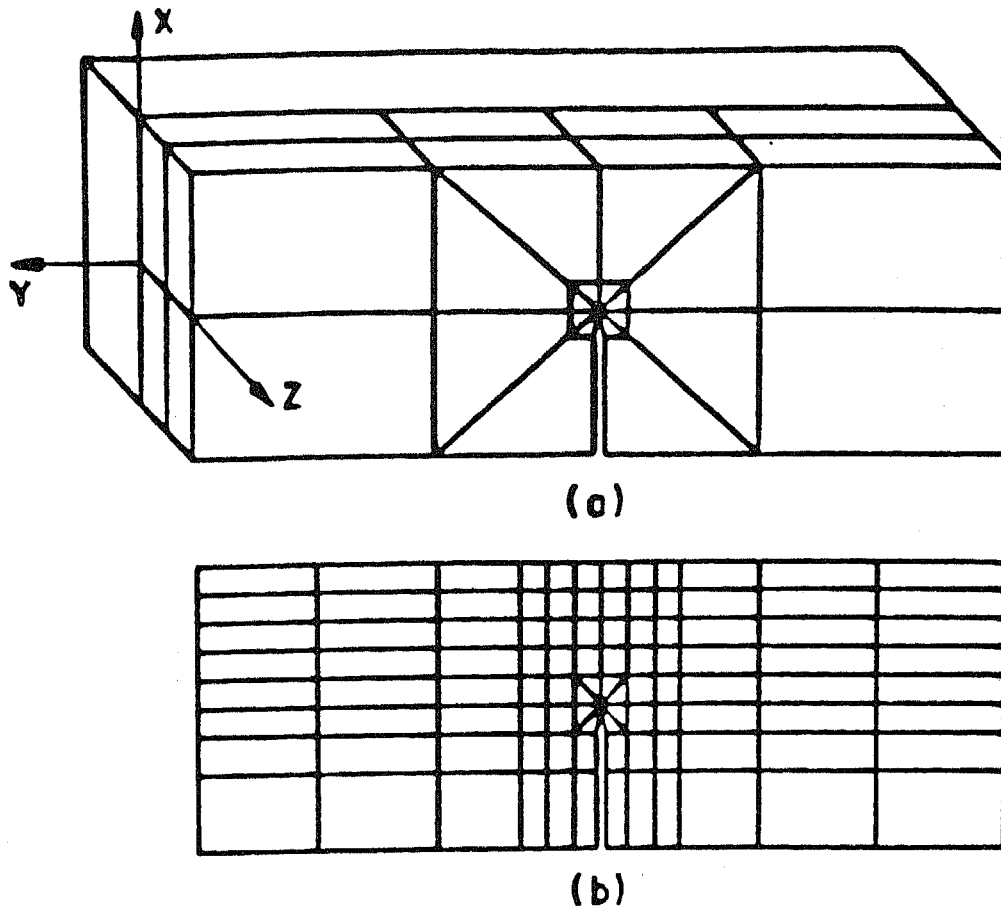


Figure 10. (a) Three-Dimensional Mesh for ASTM E-399 Standard Three-Point Bend Specimen. (b) Two-Dimensional Mesh for the Same Structure.

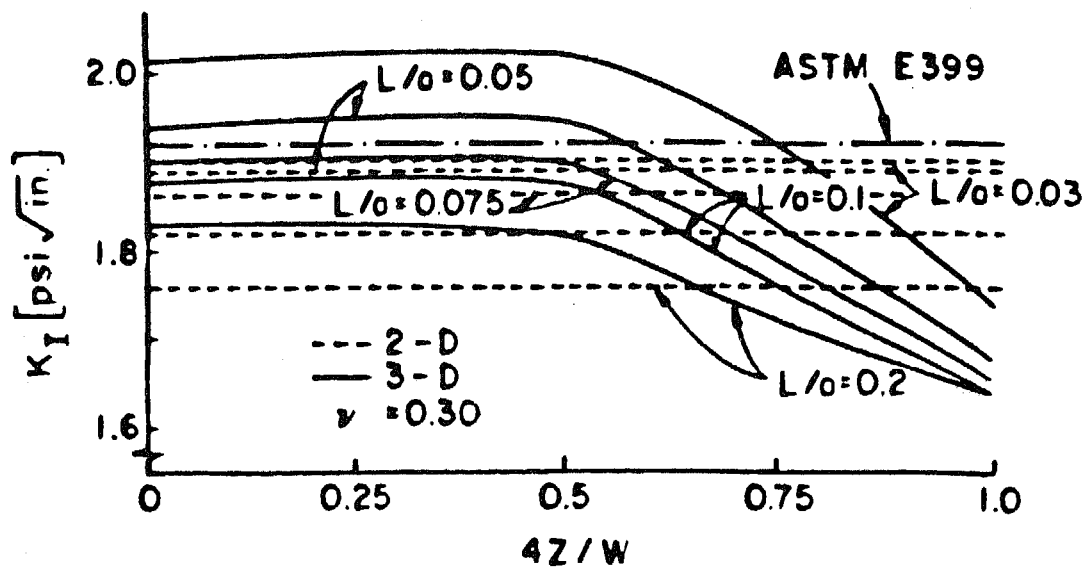


Figure 11. Comparison of 2- and 3-Dimensional Finite Element Solutions with ASTM E-399 Standard Solution.

that, other conditions being met as discussed below, engineering accuracy is assured with L/a ratios in the 0.05 to 0.15 range. Although the automatic remeshing algorithm in FEFFLAP does not include the L/a ratio as a constraint parameter, the user can interactively modify the size of crack tip elements after remeshing, by dragging nodes and changing common diagonal orientation of adjacent triangular elements.

A second mesh characteristic which can strongly influence accuracy is the number of singular elements positioned around the crack tip. More specifically, the maximum circumferential angle subtended by any of these elements must be limited to less than about 60 degrees, with 45 degrees seeming to be an optimal choice. The reason for this is that the theoretical circumferential variation in displacement is trigonometric and has a number of inflection points; the quarter-point elements are piecewise quadratic in their approximation to this variation. Take the three-point bend problem of Figure 10 and the results shown in Figure 11, for example: if the number of singular elements around the crack tip were reduced from 8 to 6 (4 to 3 using the symmetry of the problem), the error for any given value of L/a would double, approximately. Although the result might still be acceptable for small L/a , one would, of course, rather use the largest L/a practicable so that the mesh is minimally disturbed by the crack tip. The remeshing algorithm in FEFFLAP automatically varies the number of elements around the crack tip as a function of a user specified subtended angle.

With proper care in near-tip meshing with quarter-point modified elements, Equations (12) can easily produce engineering accuracy in stress intensity factor calculations.

3.2.1.2 Mixed-mode interaction formulas

As outlined above, the next step after calculation of stress intensity factors is the assessment of crack stability and angle of incipient propagation. This is done using a mixed-mode fracture initiation theory. Details of and comparisons among a number of such theories are given in references [1-3]. Only the final formulations for the three theories available in FEFFLAP are discussed here.

In the first theory the parameter governing fracture initiation is the maximum circumferential tensile stress, $\sigma_{\theta\max}$, near the crack tip [29]. Given a crack under mixed-mode conditions, the stress state near its tip can be expressed in polar coordinates as:

$$\begin{aligned}\sigma_r &= \frac{1}{\sqrt{2\pi r}} \cos \frac{\theta}{2} [K_I(1 + \sin^2 \frac{\theta}{2}) + \frac{3}{2} K_{II} \sin \theta - 2K_{II} \tan \frac{\theta}{2}] + \dots \\ \sigma_\theta &= \frac{1}{\sqrt{2\pi r}} \cos \frac{\theta}{2} [K_I \cos^2 \frac{\theta}{2} - \frac{3}{2} K_{II} \sin \theta] + \dots \\ \tau_{r\theta} &= \frac{1}{\sqrt{2\pi r}} \cos \frac{\theta}{2} [K_I \sin \theta + K_{II}(3 \cos \theta - 1)] + \dots\end{aligned}\tag{13}$$

These stress components are shown in Figure 12. The $\sigma_{\theta\max}$ theory states that:

- crack extension starts at the crack tip, in a radial direction.
- crack extension starts in a plane normal to the direction of greatest tension, i.e., at θ_0 such that $\tau_{r\theta} = 0$.
- crack extension begins when $\sigma_{\theta\max}$ reaches a critical, material constant value.

The theory is stated mathematically using Equations (13).

$$\sigma_\theta \sqrt{2\pi r} = \text{constant} = \cos \frac{\theta_0}{2} [K_I \cos^2 \frac{\theta_0}{2} - \frac{3}{2} K_{II} \sin \theta_0] = K_{Ic}\tag{14}$$

$$\text{or } 1 = \cos \frac{\theta_0}{2} \left[\frac{K_I}{K_{Ic}} \cos^2 \frac{\theta_0}{2} - \frac{3}{2} \frac{K_{II}}{K_{Ic}} \sin \theta_0 \right]\tag{15}$$

$$\text{and, } \tau_{r\theta} = 0 \quad \cos \frac{\theta_0}{2} [K_I \sin \theta_0 + K_{II}(3 \cos \theta_0 - 1)] = 0.\tag{16}$$

Equations (15) and (16) are the parametric equations of a general fracture initiation locus in the K_I - K_{II} plane, shown in Figure 13. Also, the direction of the initial fracture increment, θ_0 , can be found from equation (16) which gives,

$$\begin{aligned}\theta_0 &= \pm \pi \text{ (trivial)} \\ K_I \sin \theta_0 + K_{II} (3 \cos \theta_0 - 1) &= 0.\end{aligned}\tag{17}$$

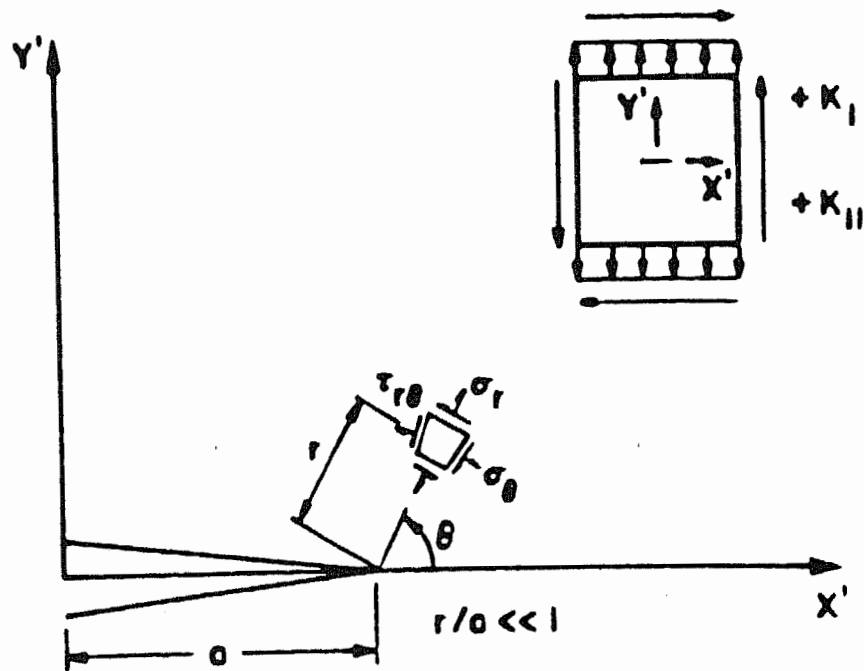


Figure 12. Crack-Tip Stress Components and Stress-Intensity Factor Sign Convention.

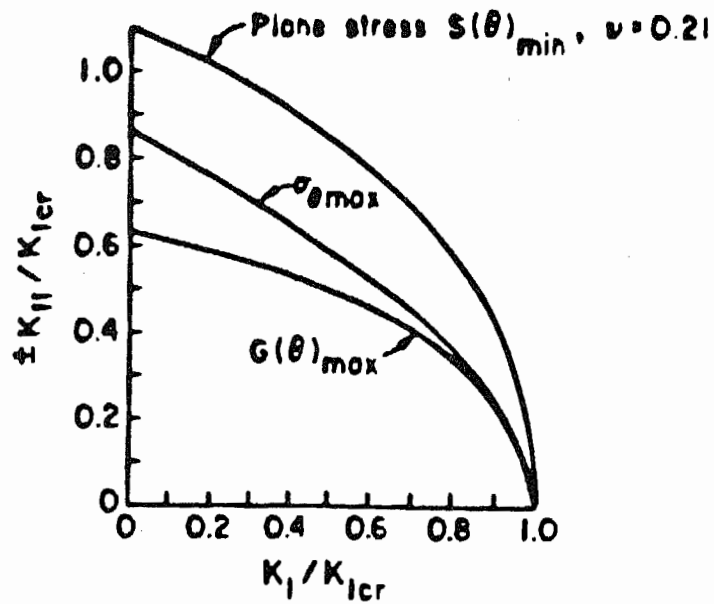


Figure 13. Fracture Initiation Loci for General Two-Dimensional Loading.

In summary, the governing equations of the $\sigma_{\theta_{\max}}$ theory are (15) and (17). Algorithmically, the stress intensity factors for a given crack tip location and loading are first substituted into Equation (17) to obtain the new angle of propagation, θ_0 . The stress intensity factors and the angle θ_0 are then substituted into Equation (15). If it is not satisfied, the stress intensity factor pair plots either within or outside the fracture locus shown in Figure 13. If within, then that crack cannot propagate without some increase in stress intensity factors. If outside, then the crack is unstable and can continue to propagate until it reaches a free surface or until the stress intensity factor pair returns to within the locus.

In the second mixed-mode fracture initiation theory, the parameter governing fracture initiation is the minimum strain energy density $S(\theta)_{\min}$, near the point of initiation [30-32].

The strain energy density variation at a distance r from a crack tip is [30]

$$\frac{\partial U}{\partial V} = \frac{1}{r} \left(\frac{a_{11} K_I^2 + 2a_{12} K_I K_{II} + a_{22} K_{II}^2}{\pi} \right) \quad (18)$$

where,

$$\begin{aligned} a_{11} &= \frac{1}{16G} [(1 + \cos \theta)(\kappa - \cos \theta)] \\ a_{12} &= \frac{\sin \theta}{16G} [2 \cos \theta - (\kappa - 1)] \\ a_{22} &= \frac{1}{16G} [(\kappa + 1)(1 - \cos \theta) + (1 + \cos \theta)(3 \cos \theta - 1)]. \end{aligned} \quad (19)$$

If the quantity in parentheses in Equation (18) is called S , i.e.,

$$\frac{\partial U}{\partial V} = \frac{S}{r_0}, \quad (20)$$

it can be seen that, at a constant value of r , S is the varying intensity of the strain energy density around the crack tip.

The $S(\theta)_{\min}$ theory proposes that:

- Crack extension occurs in the direction along which $\partial U/\partial V$ possesses a minimum value, i.e., θ_0 such that,

$$\frac{\partial S}{\partial \theta} = 0 \quad \frac{\partial^2 S}{\partial \theta^2} \geq 0. \quad (21)$$

- Crack extension occurs when $S(\theta_0)$ reaches a critical, material value, S_c .
- $S(\theta)$ is evaluated along a contour $r = r_0$, where r_0 is a material constant.

By combining the last two points it can be seen that,

$$\left(\frac{\partial U}{\partial V}\right)_c = \frac{S_c}{r_0}. \quad (22)$$

That is, specifying S_c and r_0 to be material constants is equivalent to specifying a material critical strain energy density. A relationship between S_c and fracture toughness can be obtained in the following manner. For $K_{II} = 0$, Equation (21) predicts that $\theta_0 = 0^\circ$. Then, for $K_I = K_{Ic}$, equating Equation (22) to Equation (18) yields,

$$S_c = \frac{(\kappa-1)K_{Ic}^2}{8\pi G} \quad (23)$$

A fracture initiation locus in the K_I - K_{II} plane is then obtained from,

$$\frac{S_c}{r_0} = \frac{1}{\pi r_0} (a_{11}K_I^2 + 2a_{12}K_I K_{II} + a_{22}K_{II}^2)$$

or

$$1 = \frac{8G}{(\kappa-1)} \left[a_{11} \left(\frac{K_I}{K_{Ic}} \right)^2 + 2a_{12} \frac{K_I K_{II}}{K_{Ic}} + a_{22} \left(\frac{K_{II}}{K_{Ic}} \right)^2 \right] \quad (24)$$

where θ_0 is obtained from the conditions Equation (21).

Although the direction $\theta_0 = 0^\circ$ for fracture initiation in pure Mode I is not elasticity constant dependent, θ_0 for all other cases is a function of Poisson's ratio in the $S(\theta)_{\min}$ theory.

To summarize, Equations (21) and (24) govern the $S(\theta)_{\min}$ theory. The algorithm begins with satisfaction of Equation (21) to obtain θ_0 . This angle and the stress intensity factors are then substituted into Equation (24). The crack stability implications are then the same as outlined in the section describing the $\sigma_{\theta_{\max}}$ theory.

The third theory available in FEFFLAP for mixed-mode interaction is known as the maximum strain energy release rate theory [33]. It states that "a crack subjected to mixed-mode loading will grow in the direction θ (Fig. 12) for which the energy release rate $G(\theta)$ is maximal over those values of θ for which $K_I(\theta)$ is positive. The crack will start to grow when this maximum rate reaches a critical material value G_c , which can be expressed in terms of K_{IC} " [1,33]. Given a crack tip subjected to arbitrary K_I and K_{II} , the rate of energy release associated with infinitesimal extension of the crack tip in a direction θ is:

$$G(\theta) = \frac{4}{E} \left(\frac{1}{3+\cos^2\theta} \right)^2 \left(\frac{1-\theta/\pi}{1+\theta/\pi} \right)^{\theta/\pi} [(1+3\cos^2\theta)K_I^2 + 8 \sin\theta\cos\theta K_I K_{II} + (9-5\cos^2\theta)K_{II}^2] \quad (25)$$

Note that the stress-intensity factors (SIF's) at the tip of the infinitesimal branch crack are not the same as the SIF's at the crack tip from which it springs. The first are related to the second by:

$$K_I(\theta) = \left(\frac{4}{3+\cos^2\theta} \right) \left(\frac{1-\theta/\pi}{1+\theta/\pi} \right)^{\theta/2\pi} [K_I \cos \theta + \frac{3}{2} K_{II} \sin \theta] \quad (26)$$

$$K_{II}(\theta) = \left(\frac{4}{3+\cos^2\theta} \right) \left(\frac{1-\theta/\pi}{1+\theta/\pi} \right)^{\theta/2\pi} [K_{II} \cos \theta - \frac{1}{2} K_I \sin \theta]$$

The fracture initiation locus predicted by the $G_{\theta_{\max}}$ theory is:

$$1 = 4 \left(\frac{1}{3 + \cos^2 \theta_o} \right)^2 \left(\frac{1 - \theta_o / \pi}{1 + \theta_o / \pi} \right)^{\theta_o / \pi} \left[(1 + 3 \cos^2 \theta_o) \left(\frac{K_I}{K_{Ic}} \right)^2 + 8 \sin \theta_o \cos \theta_o \frac{K_I K_{II}}{K_{Ic}^2} + (9 - 5 \cos^2 \theta_o) \left(\frac{K_{II}}{K_{Ic}} \right)^2 \right] \quad (27)$$

To summarize, Equations (25) to (27) govern the $G_{\theta_{\max}}$ theory. The algorithm begins with finding the θ_o which maximizes $G(\theta)$ in equation (25) and which at the same time, gives a positive $K_I(\theta)$ in Equation (26). Even though there can be several local stationary values for θ_o , there is only one which make K_I positive in Equation (26). This θ_o and the SIF's of the original crack tip are then substituted in Equation (27). The crack stability implications are then the same as outlined in the section describing the $\sigma_{\theta_{\max}}$ theory.

Figure 13 shows that predictions from the $G_{\theta_{\max}}$ theory are systematically conservative when compared to those of the other two theories. However, the experience of the authors is that crack trajectory predictions are not very different between the three theories, as embodied in FEFFLAP. So, the $\sigma_{\theta_{\max}}$ approach is usually preferred because it is computationally more efficient.

Of course, in a quasi-static crack propagation analysis the governing equations for one of the theories would be applied at the end of each growth step or load step for each crack tip. It may not be necessary to increase loads to bring the stress intensity factor of a previously stable crack tip onto the fracture locus. The propagation of another crack may cause the same effect. Algorithmically, this implies that the interaction factor for each crack tip, the right-hand-side of Equation (15), (24), or (27) be updated in memory after each crack or load increment. Depending on the mode of interaction between the program and the user, the former or the latter will use the interaction factors to decide which one or more of the crack tips should be propagated in a given fracture step.

3.2.1.3 Predicting crack increment length

The third and last step in the crack propagation algorithm according to the linear model is prediction of the load change required to drive a crack a specified distance. Alternatively, a load change may be specified and the corresponding crack increment sought.

The fundamental principle here is that a crack, once initiated, will continue to propagate as long as there is sufficient energy or, equivalently, effective stress intensity, available. Effective stress intensity, K^* , here refers to a mixed-mode case and is the combination of Mode I and II stress intensity factors required by the particular mixed-mode theory in use. The right-hand sides of Equations (15), (24), and (27) can, therefore, be viewed as normalized effective stress intensity factors.

A number of possible stability cases must be considered in creating an algorithm for predicting crack increment length. Some examples will be considered here with reference to Figures 14 and 15. Assume first that propagation along some predicted direction θ_0 is being investigated.

Case 1: Effective stress intensity increases monotonically with crack length, curve OA in Figure 14. If the initial crack length is less than a_i , no propagation occurs. For $a = a_i$, propagation can occur and it will continue at $P = P_i$; that is, a condition for local instability has been met. Of course, an algorithm could be written which would place such a scenario in displacement or crack-length control: a crack increment, Δa , could be specified and the load decrement required to just bring the crack tip to $a_i + \Delta a$ could be computed. This situation is depicted by curve OA' in Figure 14. To compute P_{i+1} recall that LEFM specifies that at instability,

$$K_{Ic} = \alpha_i P_i \sqrt{a_i} = \alpha_{i+1} P_{i+1} \sqrt{a_{i+1}} \quad (28)$$

where, α = factor depending on geometry and interaction theory. Therefore,

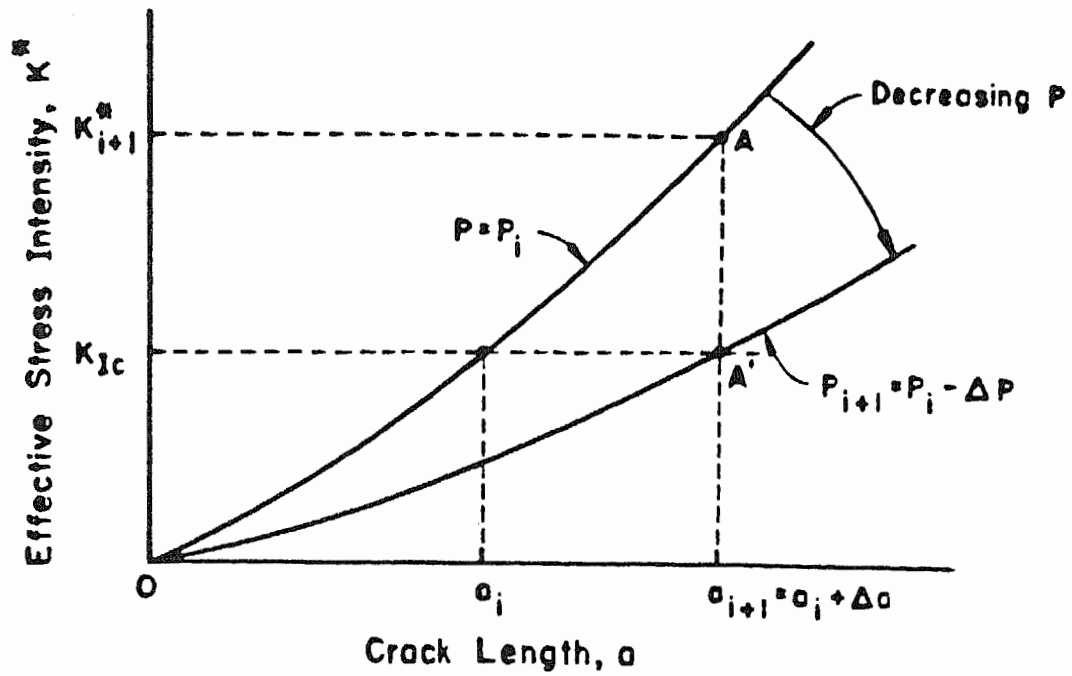


Figure 14. Stress-Intensity Factor Variation for Load-Unstable Propagation.

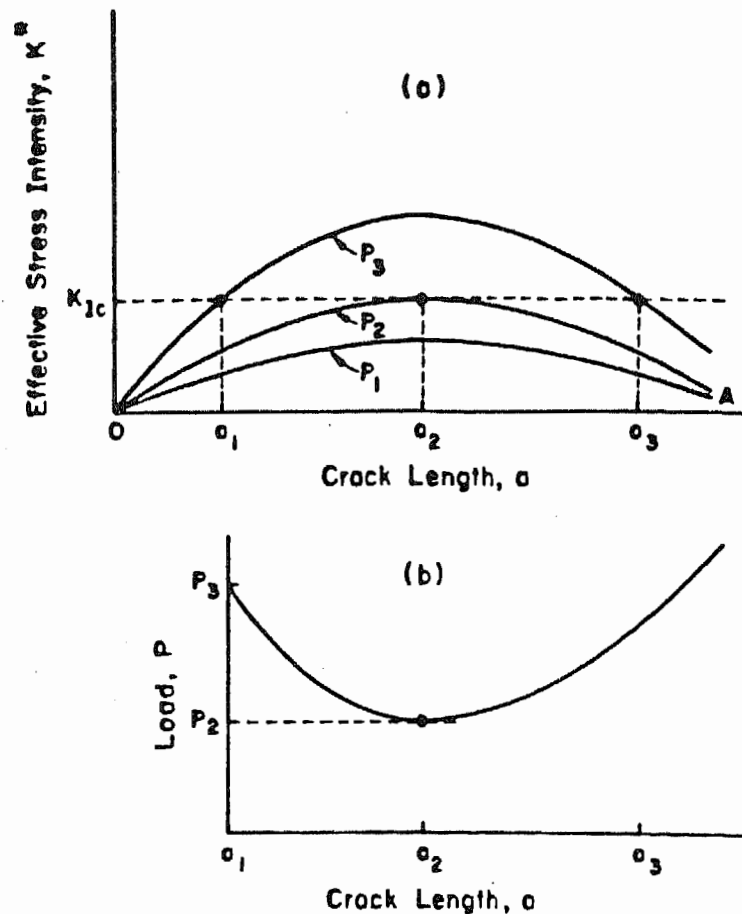


Figure 15. (a) Stress-Intensity Factor Variation for Case 2.
(b) Corresponding Load Variation.

$$P_{i+1} = \frac{\alpha_i}{\alpha_{i+1}} P_i \sqrt{\frac{a_i}{a_{i+1}}} \quad (29)$$

Equation (29) is only directly useful, however, if the α_{i+1} coefficient is known at step i . For arbitrary problems, this is certainly not the case. An alternative is to propagate the fracture an amount Δa (in the direction θ_0) and compute K_{i+1}^* at load level P_i . The new load level required to bring the crack tip to its new location is then (Fig. 14):

$$P_{i+1} = \left(\frac{K_{Ic}}{K_{i+1}^*} \right) P_i \quad (30)$$

Case 2: Effective stress intensity increases, reaches a maximum value, and then decreases with increasing crack length, curve OA in Figure 15a. For the value of K_{Ic} shown and at load level P_1 , no crack propagation is possible. At load level P_2 , propagation is possible only at crack length $a = a_2$, but the corresponding, theoretical crack increment length is $\Delta a = 0$. At load level P_3 , propagation can occur for a crack of length a_1 , and it would be unstable in load control. Again, as in Case 1, the crack of initial length a_1 could be propagated stably to length a_2 by decreasing the load incrementally from level P_3 to level P_2 , as shown in Figure 15b.

For crack lengths longer than a_2 , crack propagation is stable in the load control sense. An effective stress intensity monotonically decreasing with increasing crack length implies that a monotonically increasing load is required for continued propagation. In Figure 15, it can be seen that if the load is again increased to P_3 , propagation to crack length a_3 is possible. If one is starting with crack length a_1 , and load level P_3 (Figure 15), the prediction technique is the same as described under Case 1: propagate the crack an amount Δa in the direction θ_0 at load P_3 , compute the effective stress intensity for the new crack length, and apply equation (30). Suppose, however, that one is at load level P_2 and crack length a_2 . The same algorithm can still be used: the only difference is that the quantity in parentheses in equation (30) will now always be less than one.

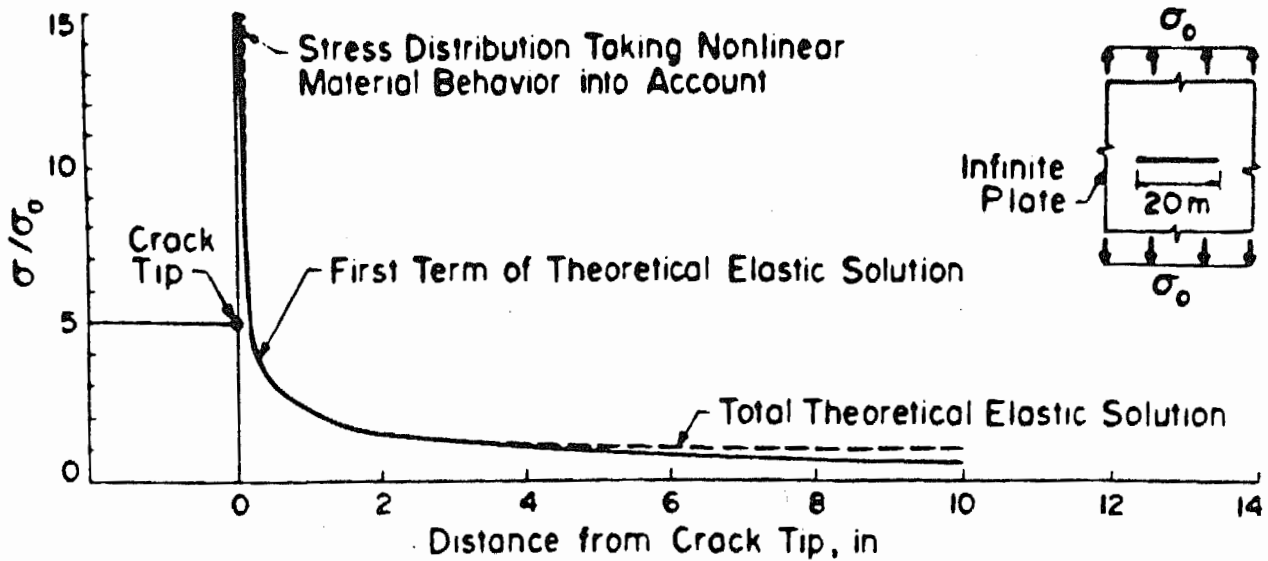
The reverse of Case 2 is also possible: effective stress intensity can at first decrease and then begin to increase with increasing crack length [34]. This situation is handled by the techniques described in Cases 1 and 2.

A number of alternative numerical techniques for crack increment length prediction are available [1,3,29,35]; some are more approximate than others. The simple technique described here is theoretically exact for pure Mode I, colinear propagation. However, any numerical technique which employs finite, straight crack increments to model curvilinear propagation will be approximate. The error depends on the specified length of the fracture increment. The analogy here is with dynamic analysis where the time step controls accuracy and stability of the solution. Experience with FEFLLAP indicates that predicted trajectories may oscillate about an average path, due to the influence of K_{II} , if too large fracture increments are allowed.

3.2.2 The Nonlinear Model

3.2.2.1 The process zone

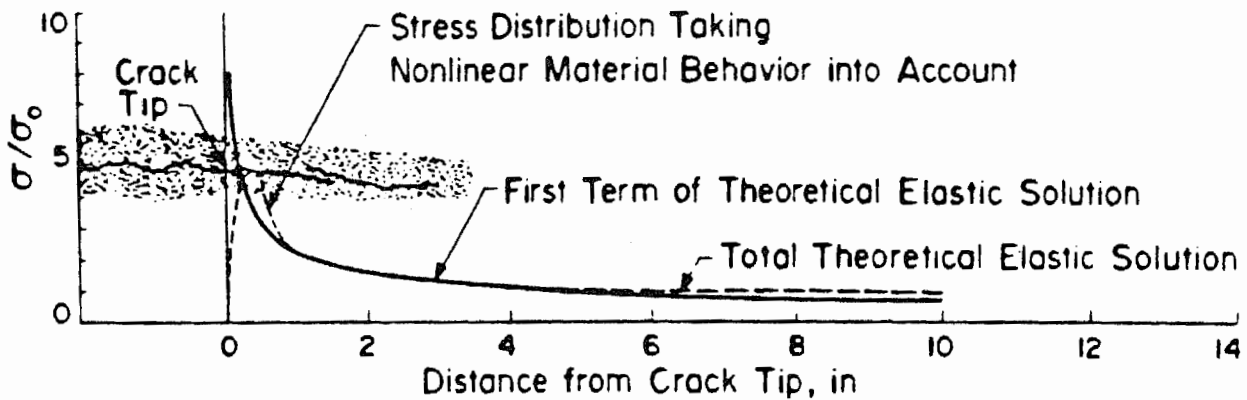
Whether linear elastic fracture mechanics is appropriate for cracking in geomaterials depends upon the nature of the process zone. Theoretically, a K_{Ic} approach is valid if the size of the process zone is small compared to the size of the area in which the singular term in the theoretical stress distribution is the dominant contribution to the stress field. This situation is investigated using the infinite plate problem of Figure 16 which shows the theoretical singular term contribution to the stress component normal to the crack plane at incipient instability, for three materials (steel, granite, and concrete). The process zones clearly affect the stress redistribution. For the metal example shown in Figure 16a, a K_{Ic} approach to fracture initiation would be valid. A K_{Ic} approach also has been shown to be applicable to many rocks. Figure 16b shows that while the process zone is much larger for this granite, the singular term still dominates.



(a) AISI 4340 Steel

$$f_y = 2 \times 10^5 \text{ psi } (1.4 \times 10^6 \text{ kPa})$$

$$K_{Ic} = 75 \times 10^3 \text{ psi } \sqrt{\text{in}} \text{ } (2600 \times 10^3 \text{ kPa } \sqrt{\text{mm}})$$



(b) Westerly Granite

$$\sigma_t = 2000 \text{ psi } (13.8 \times 10^3 \text{ kPa})$$

$$K_{Ic} = 2300 \text{ psi } \sqrt{\text{in}} \text{ } (7.9 \times 10^4 \text{ kPa } \sqrt{\text{mm}})$$

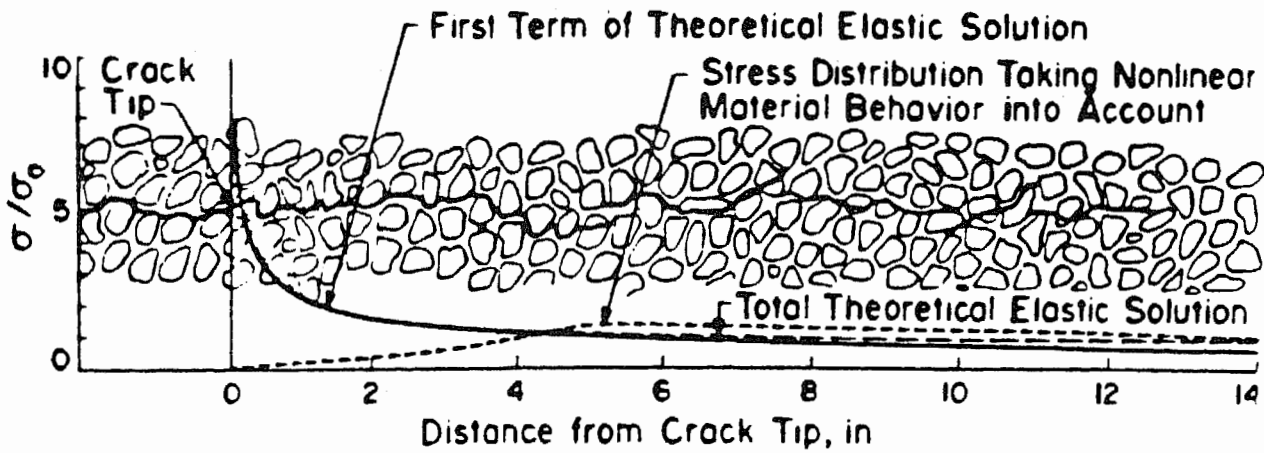
Figure 16. Comparison of Approximate Near-Tip Stress Distributions for Three Materials.

A number of recent investigations [19,20,22,24,36] have shown that these situations are quite different from that which occurs in concrete and some rocks. Figure 16c qualitatively represents process zone length in concrete, as determined by testing [19,22]. In tests on unreinforced concrete beams, stresses were still being carried over what appeared to be a visible crack. This confirmed previous experimental observations [37]: what appeared as a crack on a particular viewing surface of a specimen was in fact a "fictitious" crack in the fracture mechanics sense [24]; even though a discrete, visible crack was seen to exist on the specimen surface, this crack was not fully formed through the specimen thickness. High volumetric stresses in the process zone of concrete cause microcracking, which, when in sufficient quantity, is visible as an apparent crack on the surface. If the crack tip is viewed as the point behind which no stress is transmitted, the process zone in Figure 16c is seen to extend a relatively large distance in front of the crack tip. At the scale of the example problem, it is obvious that the singular stress term has little to do with the stress at the tip of the crack.

The stress state in the process zone in rocks and concrete is presumed to depend on the post-peak stress-strain response in tension. Such relationships have been measured [17,36,37] and have been incorporated into the process zone model in Figure 17 and implemented into FEFFLAP [21,23].

3.2.2.2 Stress versus COD models

It has been observed in direct tension tests [22,36] that microcracks, though they have not yet coalesced into a continuous, through-thickness crack, can give rise to an effective crack opening displacement. Apparently, a single, continuous crack occurs when the total effective crack opening displacement reaches a characteristic value. For typical concretes this value appears to be about 0.001 inch (0.025 mm) [22,23]. Even after this amount of opening, however, stress continues to be transmitted across the crack; stress versus COD relationships have been measured in tension [22,36]. Such relationships form the basis of the discrete nonlinear cracking model available in FEFFLAP.



(c) Concrete

$$f_y = 600 \text{ psi (4134 kPa)}$$

$$K_{Ic} = 2500 \text{ psi} \sqrt{\text{in}} \text{ (} 86.8 \times 10^3 \text{ kPa} \sqrt{\text{mm}} \text{)}$$

Figure 16. Comparison of Approximate Near-Tip Stress Distributions for Three Materials (continued).

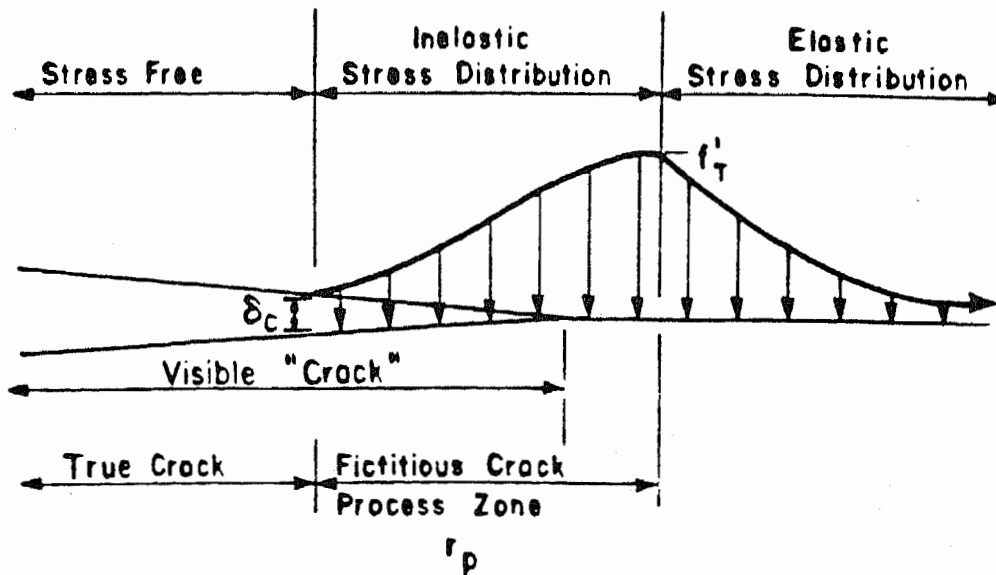


Figure 17. The Process Zone Concept for Strain-Softening Geomaterials.

Examples are shown in Figure 18. The implementation into FEFFLAP is as follows: during the automatic remeshing associated with each crack increment, the program inserts interface elements into the crack; these elements prohibit overlapping of the crack sides while allowing their relative opening and sliding. The element stiffness relationship is of the form:

$$\begin{bmatrix} \sigma_N \\ \sigma_S \end{bmatrix} = \begin{bmatrix} E_N & 0 \\ 0 & E_S \end{bmatrix} \begin{bmatrix} COD \\ CSD \end{bmatrix} \quad (31)$$

where σ_N = stress normal to crack
 σ_S = shear stress along crack
 E_N = element normal stiffness
 E_S = element shear stiffness

The elements are isoparametric and of quadratic order and can be made to possess variable normal and shear stiffness along their length. The secant normal stiffness, E_N , at any point along the crack is assigned by a relationship such as shown in Figure 19. The COD computed in a previous analysis step determines the secant E_N and, consequently, the process zone normal stress, σ_N .

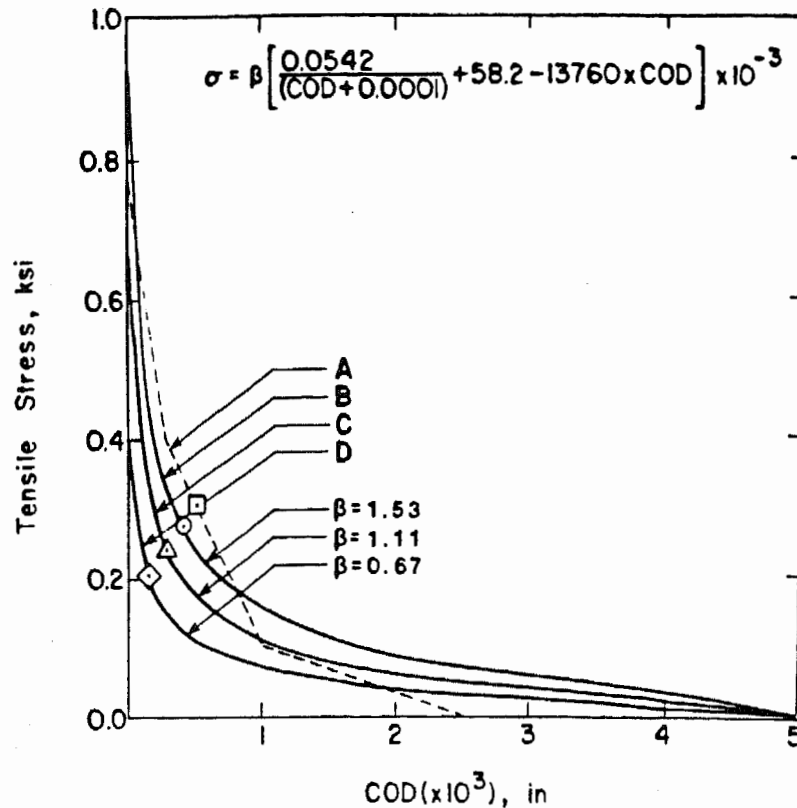


Figure 18. Typical Relationships for Normal Stress Versus Crack-Opening-Displacement for Use in the Process Zone.

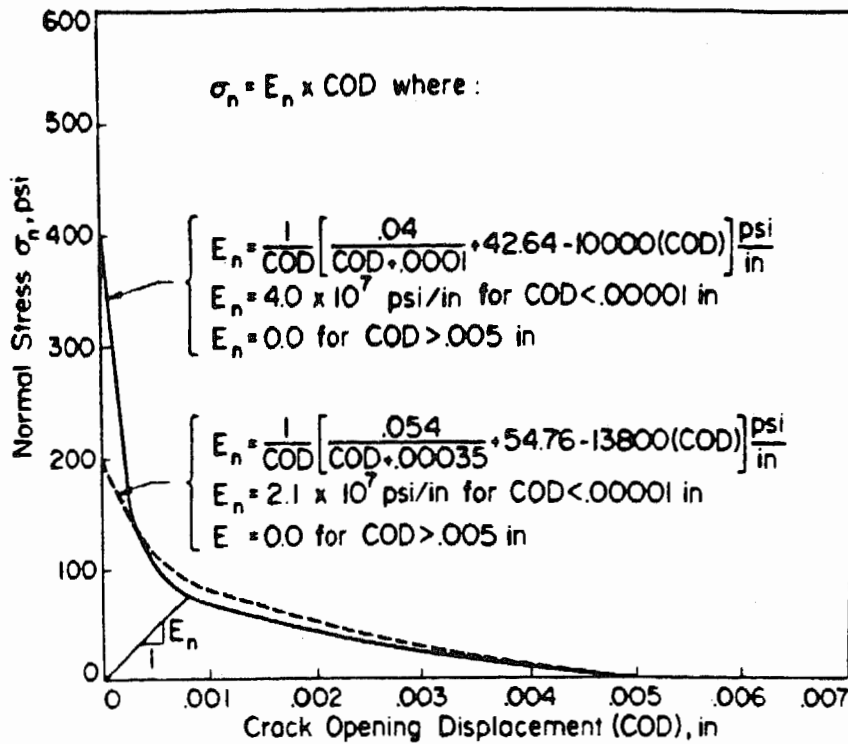


Figure 19. Typical Normal Stiffness Relationships for Interface Elements Used to Model the Process Zone.

The shear stress transferred across the crack can be modeled in a similar manner, using, for example, the relationship of Ref. [38] where the shear stress varies nonlinearly with COD and linearly with CSD (Figure 20).

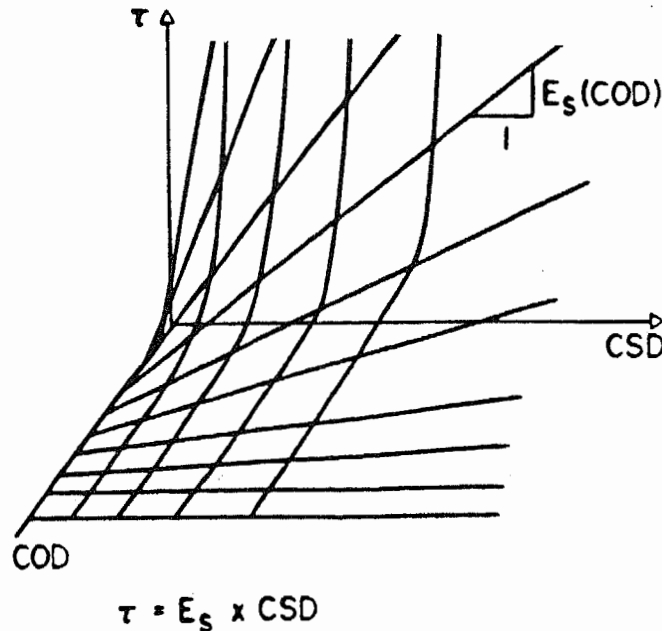


Figure 20. Qualitative Interface Element Shear Stiffness Relationship with Crack Sliding (CSD) and Crack Opening (COD) Displacements.

3.2.2.3 A nonlinear crack propagation algorithm

Nonlinear, mixed-mode crack propagation includes both shear and normal stress transfer in the process zone. Modeling in FEFFLAP is accomplished through the use of interface elements which reproduce one of the characteristic stress-versus-COD models. However, the singular elements from linear analysis are also used. They are still automatically placed at the tip of the process zone (at the tip of the fictitious crack). There are two reasons for their continued use. One wants to be able, in a single analysis, to make the transition from the nonlinear model to a linear analysis in which the process zone length becomes a negligible fraction of the total crack length. This transition is facilitated if use of the singular elements is maintained in the automatic remeshing algorithms. The second reason is that the stress intensity factors are still computed at a fictitious crack tip to confirm that they are zero. A nonzero stress intensity factor would indicate that the crack should actually have propagated beyond the existing fictitious crack tip. The nonlinear crack propagation algorithm also requires that the stress-versus-COD constitutive models be satisfied. These requirements are met in an iterative manner in the present nonlinear analysis option of FEFFLAP.

Given the typical local mesh configuration shown in Figure 21a as a starting point the following steps are performed iteratively in a crack increment:

1. Iterations are performed at the current load level until the interface model is satisfied to a specified tolerance along the entire process zone length.
2. If K_I and K_{II} calculated at the assumed fictitious crack tip are nominally zero, then the fictitious crack has not yet opened along its entire length to its assumed tip. The load may be increased by the user, and iterations again performed, until convergence is achieved (Figure 21b).
3. Step 2 is repeated until, at a given load level, K_I and/or K_{II} become nonzero after convergence (Figure 21c).

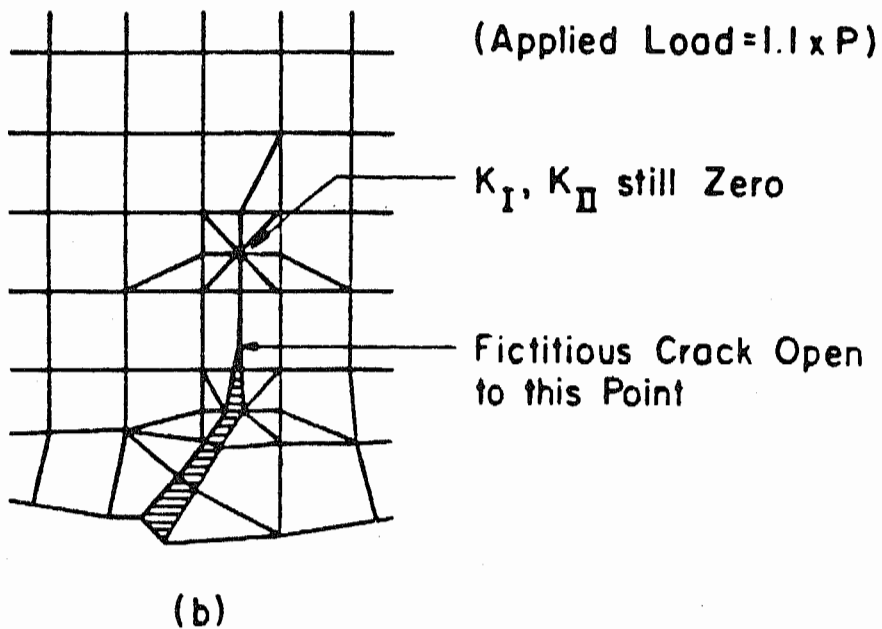
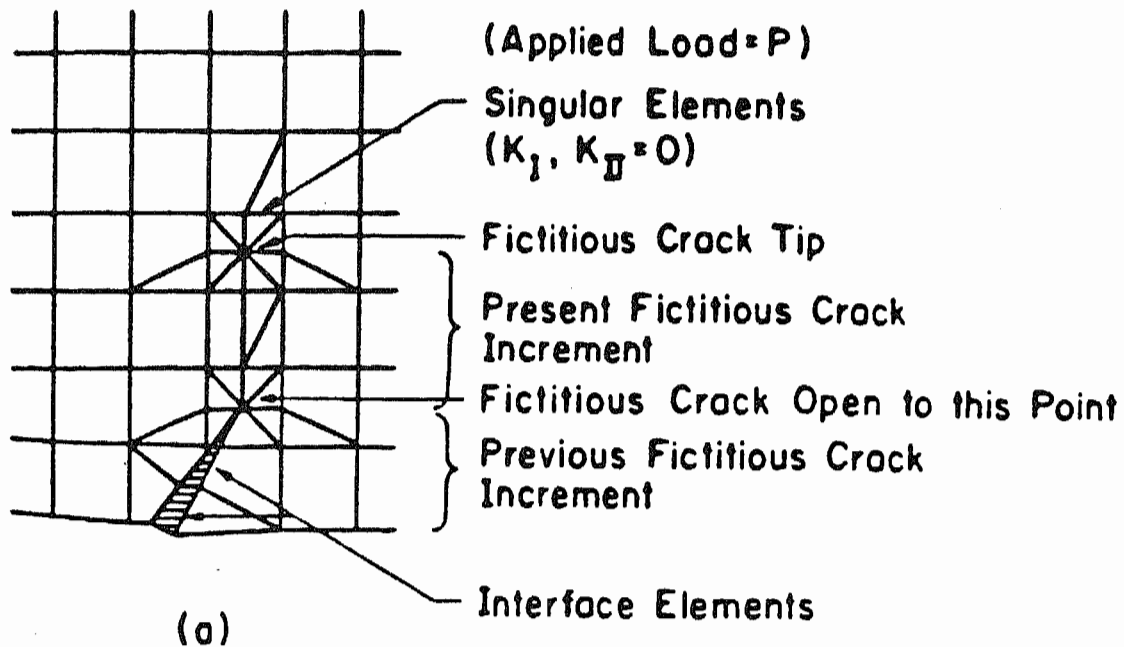


Figure 21. Schematic of Steps Involved in Mixed-Mode, Nonlinear Crack Propagation Modeling in FEEFLAP.

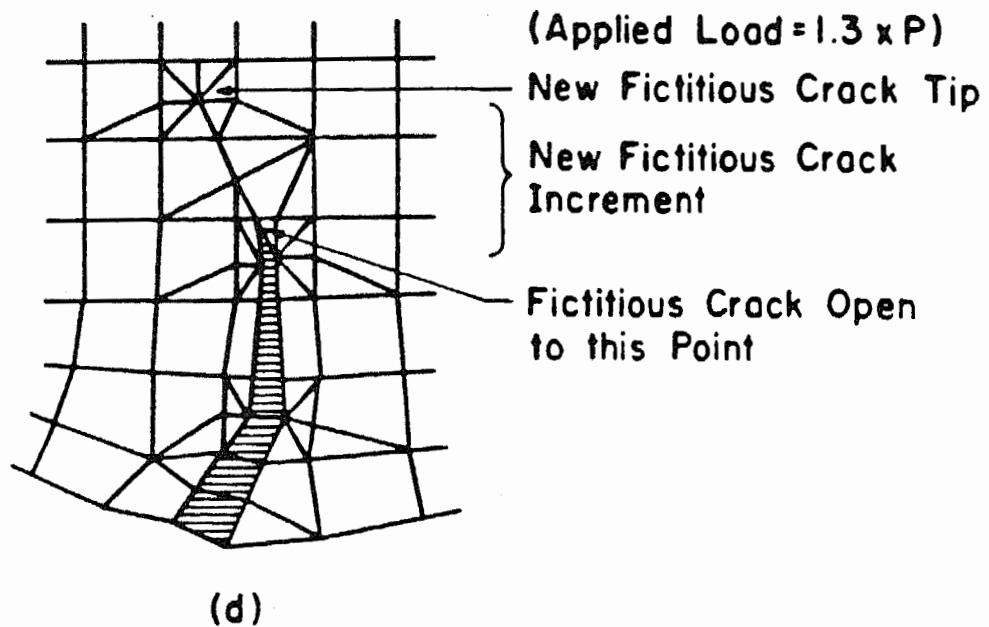
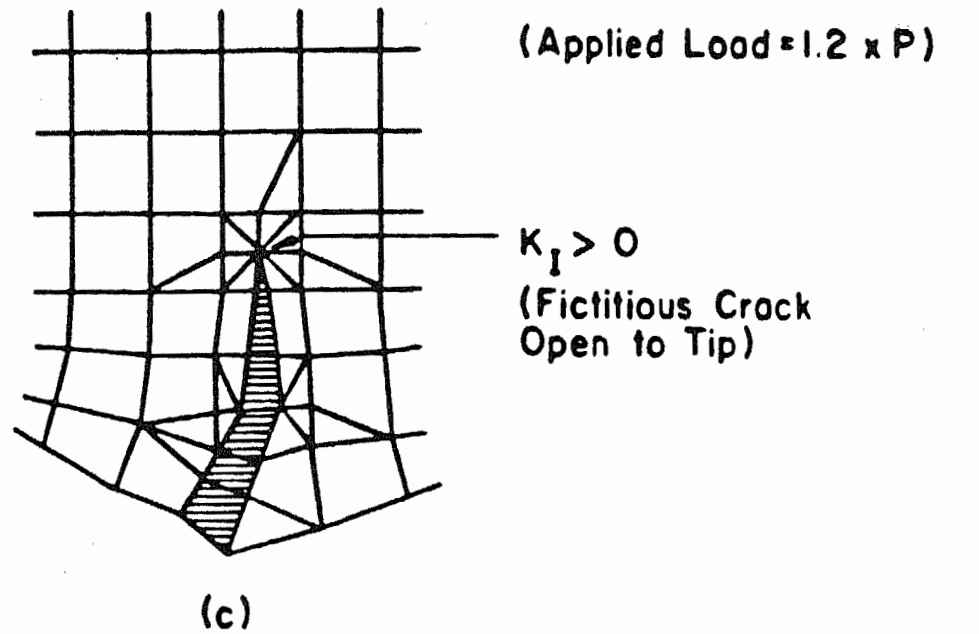


Figure 21. Schematic of Steps Involved in Mixed-Mode, Nonlinear Crack Propagation Modeling in FEFFLAP (continued).

4. Using one of the mixed-mode interaction equations (16), (21), or (25) FEFFLAP automatically calculates the direction of propagation of the next crack increment based upon the nonzero (but small) value of K_I and K_{II} . FEFFLAP then automatically remeshes (Figure 21d) to allow the fictitious crack to propagate further. The length of each fictitious crack propagation increment is prespecified by the user.
5. The process is repeated for the next crack increment (steps 1 through 4).

The nonlinear option is highly interactive. After each iteration the following quantities are displayed on the terminal screen: K_I and K_{II} for each crack, the load factor κ (Equ. 4), and values of preselected nodal displacements and reactions. In this way, the user can observe convergence trends. At any point he can decide to change the load with the present configuration, to reanalyze at the current load, or to continue to the next crack increment.

4. FLUID MECHANICS

4.1 Fluid Flow Model

The model used in FEFFLAP is a one-dimensional steady-state, incompressible, viscous fluid flow based on an LLNL-enhanced version of a U.C. Berkeley code for flow in jointed rocks [4]. Low Reynold's numbers are assumed so that the flow is laminar. The model provides for steady-state solution of flow in parallel or tapered channels such as joints, cracks, and interfaces in rock. Both flow rate and pressure boundary conditions can be specified. The fluid conductivity of individual flow elements is described by:

$$k_p = \rho g b^2 / 12 \mu \quad (32)$$

where b is the mean element aperture, ρ is the specific gravity of fluids, g the acceleration due to gravity and μ the dynamic viscosity. Then, the areal permeability along a family of parallel such fractures is proportional to b^3 . The merits and limitations of this so-called "cubic law" model have been discussed at length by others [40,41].

The governing differential equation for flow is

$$\frac{\partial}{\partial \ell} \left(k_p \frac{\partial h}{\partial \ell} \right) + q = 0 \quad (33)$$

where h is head, q is flow rate and ℓ is the spatial coordinate. A finite element formulation is employed via the calculus of variations to produce 2-node flow elements which have a linear relationship between flow rate and head (or pressure). Flow rate is determined from equation (33) and the pressure in the fluid is obtained from the finite element solution. Hence the pressure that is applied on the channel walls is known and is then used as a boundary condition in the structural model.

Several improvements were made in the original flow model [4] to bring it to its current state. First, extensive programming was done to generate the flow nodes and elements automatically at each stage of crack propagation. This was necessary because new joint elements are created as cracks extend; therefore, new flow nodes and elements must be accounted for. In addition, cracks can intersect existing joint networks so that a common flow node must be specified

at the intersection. Since flow nodes are assigned according to increasing structural joint number and the initial flow boundary conditions are tagged to flow node numbers, an automatic shifting of boundary conditions must occur. For example, if a crack intersects the middle of the joint element numbered '4', with flow node numbers 4 and 5, a new joint element is created (the original element is bisected) and the structural element number assigned to it is one more than the highest existing element number. According to the automatic numbering system, the old node numbered 5 is now 6 and the boundary conditions assigned to node 5 must now be assigned to node 6. This is true for all flow nodes greater than 5. These operations are performed automatically in the code.

4.2 Minimum Aperture for Fluid Flow

One of the important parameters in fracture flow analysis is the minimum crack aperture for fluid flow; that is, there is an aperture below which no fluid penetration will occur. The extent of fluid penetration strongly affects fracture instability as well as angle of propagation for the static case. The minimum aperture depends on the surface tension of the fluid and on the fluid pressure. In FEFFLAP the minimum aperture is estimated from surface tension theory [42]. Essentially, the radius of curvature of the fluid front R (Figure 22) is proportional to the surface tension of the fluid and inversely proportional to the pressure in the fluid. For example, in recent fracturing tests performed on hydrostone blocks [43], the surface tension for the fracturing oil was estimated from Reference [44]. At an oil pressure of 2000 psi the minimum opening for oil penetration is about 10^{-5} inches. This model gives a maximum possible wetted length that can be pressurized during each stage of the hydrofracture process.

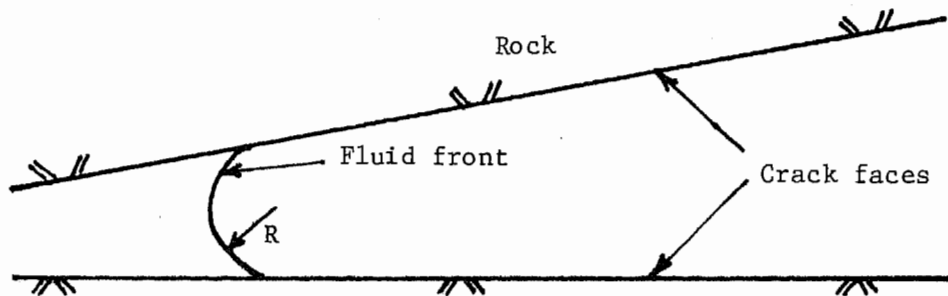


Figure 22. The Fluid Front Stops in a Narrowing Channel Due to Surface Tension.

5. PROGRAM STRUCTURE

5.1 Code Routines

FEFFLAP consists of a main routine and 105 subroutines. These are listed alphabetically in Table 1 which briefly describes the purpose of each routine. The overall structuring of the routines into the code is explained in Fig. 23. For the sake of clarity most routines are identified by groups, according to function. The main groupings in FEFFLAP are as follows:

5.1.1 Control

MAIN	.	Begins program execution and opens all input/output.
	.	Places input data in main storage vector and auxiliary arrays.
	.	Controls operation of program under non-crack propagation mode.
CRAPRO	.	Controls program in crack propagation operation mode.
	.	Controls all crack initiation and crack increment operations.
GRCURF	.	Controls all operations within a crack increment.
MODTOP	.	Controls the mesh modification operations required for crack propagation.
OPEN1	.	Control the mesh modification operations required by the
OPEN2		opening of a new crack from a node or an edge, respectively.
NPOINT	.	Controls the value of pointers used to locate data in the main storage vector.

5.1.2 Input/Output Operations

All initial data are input through MAIN, INPUT, and LOAD.

Interactive alphanumeric I/O via PLOT-10 routines (5.1.4) is initiated by MAIN, CRAPRO, GRCURF, MODTOP and OPEN1. Many routines produce output for the output file and/or the terminal. Those routines that produce only output operations are listed in Table 2.

Operation of FEFFLAP requires that a number of I/O files be available. These files, their function, and their device relationship are listed in Table 3.

TABLE 1. Subroutines Used in FEFFLAP Version 1.0.

ADD:	Adjusts number of equations for new nodes
ADILOC:	Adjusts cursor location
ARROW:	Plots arrows in stress plot
APERTUR:	Calculates initial apertures for fluid flow
BANMIN:	Control routine for mesh optimization
BANWID:	Computes bandwidth
BLKSTF:	Blocks the stiffness matrix
BMAT:	Fills b matrix (FEM routine)
BREAK:	Breaks element into 2 elements
CHKANG:	Checks if crack tip element angle is too large
CHKBND:	Checks if material number corresponds to a joint element
CRAPRO:	Control routine for crack initiation and propagation
CREAT2:	Dummy routine
DANIS:	Computes d matrix for anisotropic elements
DATER:	Dummy routine
DGREE:	Computes degree of node for bandwidth minimization
DISTAN:	Finds distance between a point and a line
DJOINT:	Computes the d matrix of joint elements
DLIN:	Computes material stiffness coefficients
DOBCRO:	Checks if and where a crack entering an element will exit
DXBMAT:	Computes dxb
ELAXS:	Determines adjacent element
ELXNOD:	Finds all elements around a node
ELXSID:	Determines adjacent element
ERROR:	Notifies user of insufficient memory
EXITIT:	Closes files and ends program
FAILUR:	Checks for condition of crack initiation
FLINDS:	Fills initial displacement array
FLOW:	Solves flow equations
FLOWBY:	Control routine for fluid flow
FNDIAM:	Computes width for bandwidth minimization
FRAINI:	Finds fracture instability and angle of propagation
GAUSS:	Initializes values for numerical integration
GRCURF:	Control routine for crack extension
GVALUE:	Determines energy release rate
IDXYRE:	Finds nearest node
INDINV:	Remembers nodes in bandwidth minimization
INPUT:	Reads most of the initial input data
INTCUR:	Draws stress intensity factor interaction curves
JACOB:	Calculates determinant and inverse of Jacobian matrix
JOINTE:	Computes stiffness matrices of joint elements
JOISTR:	Computes stresses in joint elements
LINPLO:	Draws a vector
LOAD:	Assembles the initial load array
LOCNOL:	Determines node closest to a point
LOCNO2:	Determines local node closest to a point
LODCRK:	Finds nodal loads equivalent to fluid pressure
MESHOP:	Control routine for mesh optimization
MODTOP:	Control routine for mesh modification
MONPRT:	Prints preselected nodal displacements
MONWRT:	Writes preselected nodal displacements to teletype
NODEXY:	Computes coordinates of midside nodes

NPOINT: Sets pointers for the A array
NUMBE: Numbers the graph for minimum bandwidth
NUMPLO: Plots numbers on monitor
NWODXY: Computes coordinates of midside nodes
OPEC: Initiates crack from a corner
OPEN2: Initiates crack from an element side
PDELTA: Plots load-displacement curve
PERCRK: Relocates quarter-point nodes in singular elements
PIKLVL: Chooses level structure in bandwidth minimization
PLOTT: Controls plotting routine
PLTALL: Plots whole mesh
QUARTER: Shifts midside node to quarter-point in singular elements
REAC: Calculates the reactions
REDUCE: Bandwidth minimizer
REFINE: Refines the mesh
SETUP: Computes reverse leveling for bandwidth minimization
SHAPES: Calculates shape functions
SHIFT1: Shifts pointer by one for a new degree of freedom
SHIFT2: Shifts pointer by two for new node
SHWTIP: Outlines the tips of all cracks
SIF: Computes stress intensity factors for total load
SIFN: Computes stress intensity factors due to variable load
SKDECP: Cholesky decomposition
SKSOLX: Substitution for equation solving
SKY: Control routine for solver
SKYHLP: Assembles stiffness matrix
SLICE: Separates nodes along a crack
SOLJNT: Controls nonlinear joints if no crack propagation
SORTDG: Sorts by degree of node for bandwidth minimization
STHETA: Computes sigma-theta-min interaction curve
STIFF: Computes stiffness matrices
STRESS: Computes stresses
STRINI: Calculates variable load necessary for crack initiation
TABLE: Dumps variable values if premature termination
TIMEA: Dummy routine
TIMLOG: Calculates time required for operations
TRANSD: Transforms d matrix to global coordinate system
TREE: Organizes nodes for bandwidth minimization
TRUSK: Computes stiffness matrix of truss element
TRUSS: Computes axial stress in truss element
WRTDIS: Writes displacements to output file
XADJ: Improve aspect ratios of elements around crack tip
XBNDSD: Modifies mesh as crack crosses joint element
XNEN: Crack enters element at a node and stops near a side
XNES: Crack enters element at a node and stops far from a side
XNN: Crack enters at a node and exits from a node
XNS: Crack enters at a node and exits from a side
XSE: Crack enters from a side and stops inside an element
XSN: Crack enters from a side and exits from a node
XSS: Crack enters from a side and exits from a side
XSTLND: Modifies mesh as crack crosses bond element from a node
XSTLSD: Modifies mesh as crack crosses bond element from a side
ZERADN: Zeroes coordinates of nodes adjacent to crack exit node

MAIN* ↔ INPUT

↔ CRAPRO* ↔ LOAD ↔ APERTUR

↔ BANDWIDTH MINIMIZATION ROUTINES (Table 5)

↔ FEM ROUTINES (Table 4)

↔ STRESS INTENSITY FACTOR ROUTINES (Table 6)

↔ OPEC* ↔ OPEN2* ↔ MODTOP ↔ MESH MODIFICATION (Table 7)

↔ MODTOP ↔ MESH MODIFICATION (Table 7)

↔ BANDWIDTH MINIMIZATION ROUTINES (Table 5)

↔ FEM ROUTINES (Table 4)

↔ GRCURF*

↔ MODTOP ↔ MESH MODIFICATION (Table 7)

↔ BANDWIDTH MINIMIZATION ROUTINES (Table 5)

↔ FEM ROUTINES (Table 4)

↔ STRESS INTENSITY FACTOR ROUTINES (Table 6)

↔ FLOWBY ↔ FLOW

↔ LODCRK

↔ FEM ROUTINES (Table 4)

* Graphics routines being exercised (Table 8)

Figure 23. Program Structure of FEFFLAP as it is Exercised for a Fracture Propagation Analysis.

Table 2. Subroutines for Output Operations

DATER	MONWRT	TIMLOG
ERROR	TABLE	WRTDIS
MONPRT	TIMEA	

Table 3. I/O Logical Unit Numbers Used by FEFFLAP

File No.	Function	Device
1	Restart information	Disk
2	Currently inactive	-----
3	Interactive alphanumeric input	Terminal
4	Load vector	Disk
5	Input data	Disk
6	Output listing	Disk
7	Currently inactive	-----
8	Element stiffness matrix	Disk
9,10,11	Work space for solver	Disk
20	Problem dump	Disk

Table 4. Subroutines for Standard Finite Element Analysis

BLKSTF	JACOB	SKSOLX
BMAT	JOINTE	SKY
CHKBND	JOISTR	SKYHLP
DANIS	LOAD	SOLJNT
DJOINT	LOADCRK	STIFF
DLIN	NODEXY	STRESS
DXBMAT	REAC	TRANSD
FLINDS	SHAPES	TRUSK
GAUSS	SKDECP	TRUSS

Table 5. Subroutines Used for Bandwidth Minimization

BANMIN	INDINV	REDUCE
BANWID	MESHOP	SETUP
DEGREE	NUMBE	SORTDG
FNDIAM	PIKLVL	TREE

Table 6. Subroutines for Stress-Intensity Factor Operations

FRAINI	PERCRK	SIF
GVALUE	QUARTER	STHETA

5.1.3 Structural and Flow Analyses

Subroutines for the standard finite element analyses (stiffness assembly, displacement and stress calculations) are shown in Table 4. Routines involved in bandwidth minimization are shown in Table 5 and those for stress-intensity factor operations in Table 6.

The principal mesh modification control routines (MODTOP, OPEN1, OPEN2) call a large number of additional routines which perform various functions. A list of these routines is shown in Table 7. The core of these are the "X-Routines" which create the new mesh required by the situations shown in Figure 24.

5.1.4 Graphics Operations

The control of graphic operations is performed by the routines shown in Table 8. These routines do not perform the display themselves. Rather, they call the appropriate routines from the PLOT-10 libraries described below.

FEFFLAP operates in a conversational, interactive-adaptive graphic environment. This means that there is a continuous interchange of alphanumeric information between the program and its user and that there is graphic display of intermediate results and meshes. This interchange occurs through a combination of storage-tube (hereafter referred to as "monitor") and teletypewriter interaction. Teletypewriter exchange of alphanumeric information is handled through the usual Fortran READ and WRITE statements with the teletypewriter addressed as FILE 3. All monitor displays are performed through calls to libraries of graphics subroutines. These libraries, both part of the Tektronix, Inc. PLOT-10 graphics software system, are:

- . PLOT-10 Terminal Control System (TCS), Release 3.0
- . PLOT-10 Advanced Graphics Language II (AGL), Release 1.2

The PLOT-10 routines which are currently used by FEFFLAP are listed in Table 9. These libraries are directly compatible with most Tektronix, Inc. graphic display monitors. In particular, FEFFLAP is directly compatible with the Tektronix 4010 series of display devices.

Table 7. Subroutines for Mesh Modifications

ADD	LOCNOL	XNES
BREAK	LOCNO2	XNN
CHKANG	REFINE	XNS
DISTAN	SHIFT1	XSE
DOBCRO	SHIFT2	XSN
ELAXS	SLICE	XSS
ELXNOD	XADY	XSTLND
ELXSID	XBNDSD	XSTLSD
IDXYRE	XNEN	ZERADN

Table 8. Subroutines Controlling Graphics Operations.

ADILOC	LINPLO	PLOTT
ARROW	NUMPLO	PLTALL
INTCUR	PDELTA	SHWTIP

Table 9. PLOT-10 Routines Used by FEFFLAP

ANMODE	FFORM	SLIMY
ANSTR	FINITT	SYMBL
B INITT	HLABEL	TERM
BSYMS	INITT	TINPUT
CHECK	MOVABS	TWINDO
CHRSIZ	MOVEA	VCURSR
CPLOT	MOVREL	VLABEL
DASHA	NPTS	XETYP
DRAWA	SCURSR	XMFRM
DRWABS	SEETR	YETYP
DSPLAY	SIZES	YMFRM
DWINDO	SLIMX	








SITUATION	ROUTINE
	XSS
	XSN
	XSE
	XNS
	XNN
	XNES
	XNEN

Figure 24. The Various Situations Encountered When a Crack Crosses, Stops in, or Moves Along an Edge of an Element are Addressed by the "X-Routines".

5.2 Memory Management

Data which are input or generated during the first analysis step are stored in a straightforward manner. Most data reside in a single vector, A, whose dimension, MTOT, is specified in MAIN. The vector A is an unlabeled common block. Control routine NPOINT is called at various stages of the initial analysis to compute pointers to the starting locations of the various arrays stored in A. Figure 25 shows the A-vector structure at the input stages. Additional data are arranged in labeled common blocks. A list of these blocks and the nature of their content are shown in Table 10. A relatively small amount of data are held as individual dimensioned and undimensioned variables in each routine.

FEFFLAP creates new nodes and elements as it propagates cracks. This means that arrays whose dimensions are related to the current number of nodes, NPOIN, the current number of unrestrained degrees-of-freedom, NEQ, or the current number of elements, NELEM, change size during the course of analysis. Consequently, some of the pointers for the A-vector must be updated at appropriate times. Pointers N1 through N6 (Fig. 25) remain fixed during an analysis. To accommodate growth of the arrays stored before N6, extra space is allotted to them during the data input phase. This is accomplished by setting a limit on the maximum number of nodes and elements allowed in terms of their initial numbers, i.e.,

$$\text{MELEM} = \text{maximum number of elements permitted} = 10 * \text{initial number of elements}$$
$$\text{MPOIN} = \text{maximum number of nodes permitted} = 10 * \text{initial number of nodes}$$

Note that these limits, set in MAIN, are relative, not absolute. The only limitation on the initial number of elements or nodes is the total memory available for the A-vector, MTOT. The limits on MELEM, MPOIN, and MTOT can be easily changed by modifying four statements in MAIN. In the current program version (FEFFLAP 1.0) the maximum number of interface elements is 100, and the number of non-interface elements is 300. These limits can be easily changed by modification of a few lines of the code.

Pointers from N7 onwards change value after each crack propagation step. Subroutine NPOINT performs the updating when it is called at each stage of each reanalysis. Figure 26 shows the A-vector structure at each stage of an analysis.

Memory Allocation in Principal Storage Vector A

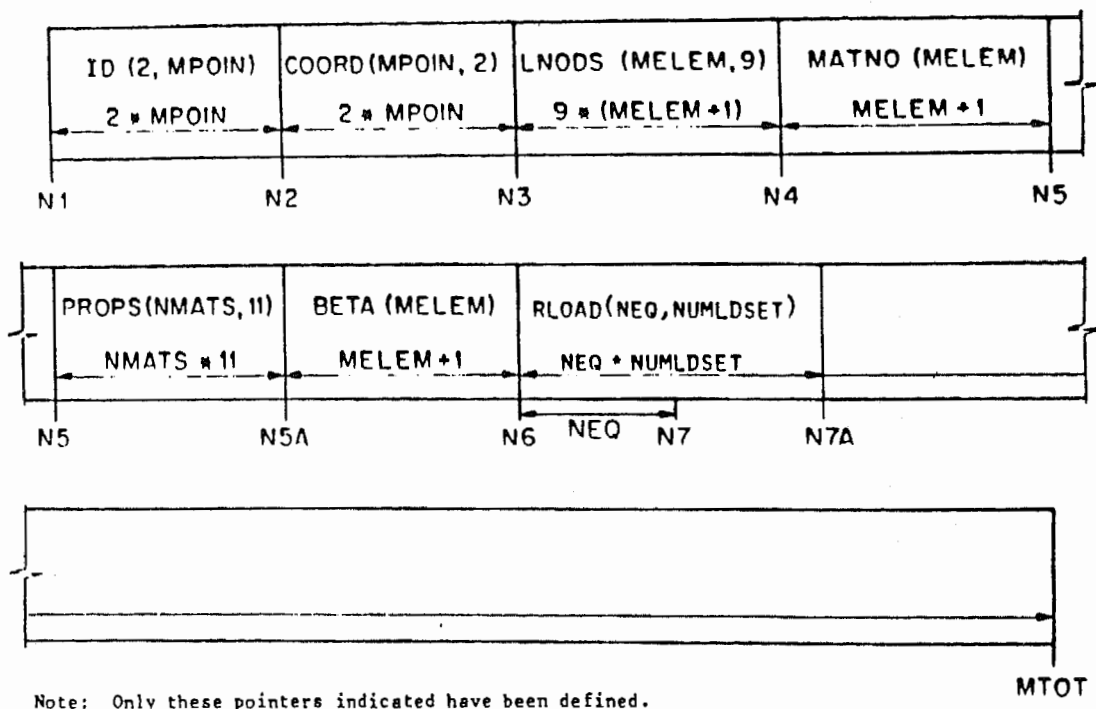


Figure 25a. On Return to MAIN from Routine INPUT.

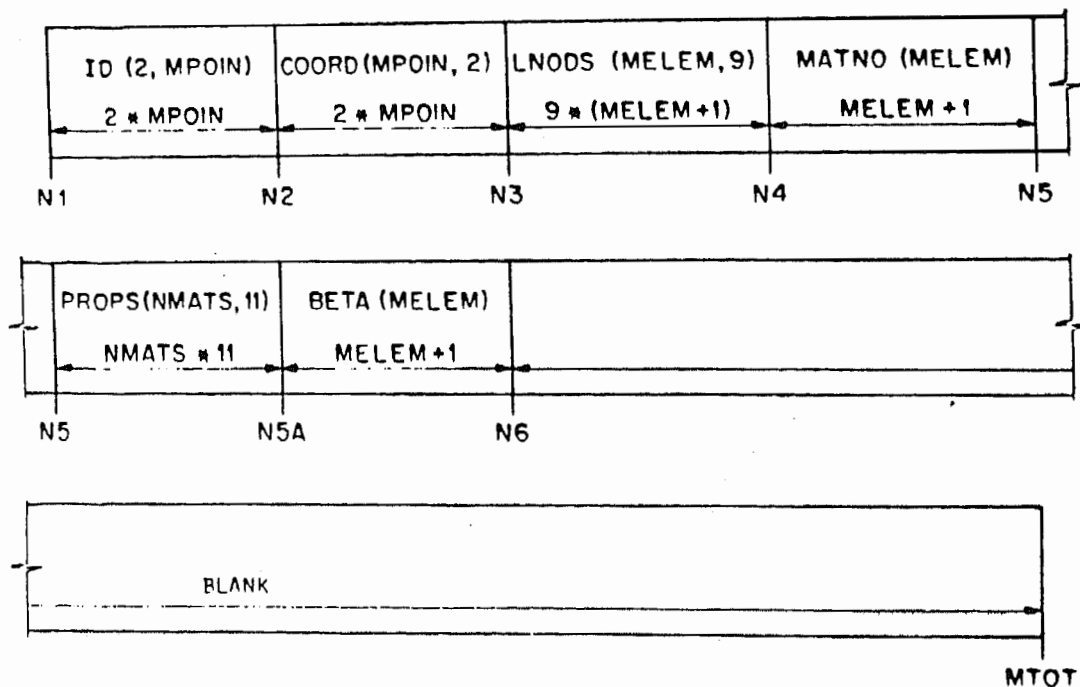


Figure 25b. On Return to MAIN or to CRAPRO from Routine LOAD.
 NEQ = Number of Unrestrained DOF's, NUMLDSET = Number of Load Sets.

TABLE 10

Labeled Common Blocks in FEFFLAP

Label	Contents
CONTRO	Principal program control parameters
BLKP	Pointers to the block of the stiffness matrix
FRACT	Crack propagation parameters
DSPLIN	Initial displacement information
INCLBL	Inclined boundary condition information
CHKLO	Temporary storage for loads and reactions
GRA	Parameters for bandwidth reduction
CC	Work area for bandwidth reduction
LVLW	Parameters for bandwidth reduction
JOINT	Initial joint element material properties
INTRST	Current joint element material properties
MATNON	Nonlinear material properties
NUMSTA	Parameters for element addition/deletion
PLOTD	Parameters for Tektronics I/O
RESULT	Information for load-displacement plot
SURF	Codes for crack propagation and an array of the material type each crack tip is in
SOLT	Parameters used by the solver
WORKI	Matrices for element stiffness formation
XSYS	Global stiffness storage parameters
YNGEL	Gauss point values of Young's modulus and Poisson's ratio
XPRPDL	Experimental load deflection data

Memory Allocation in Principal Storage Vector A

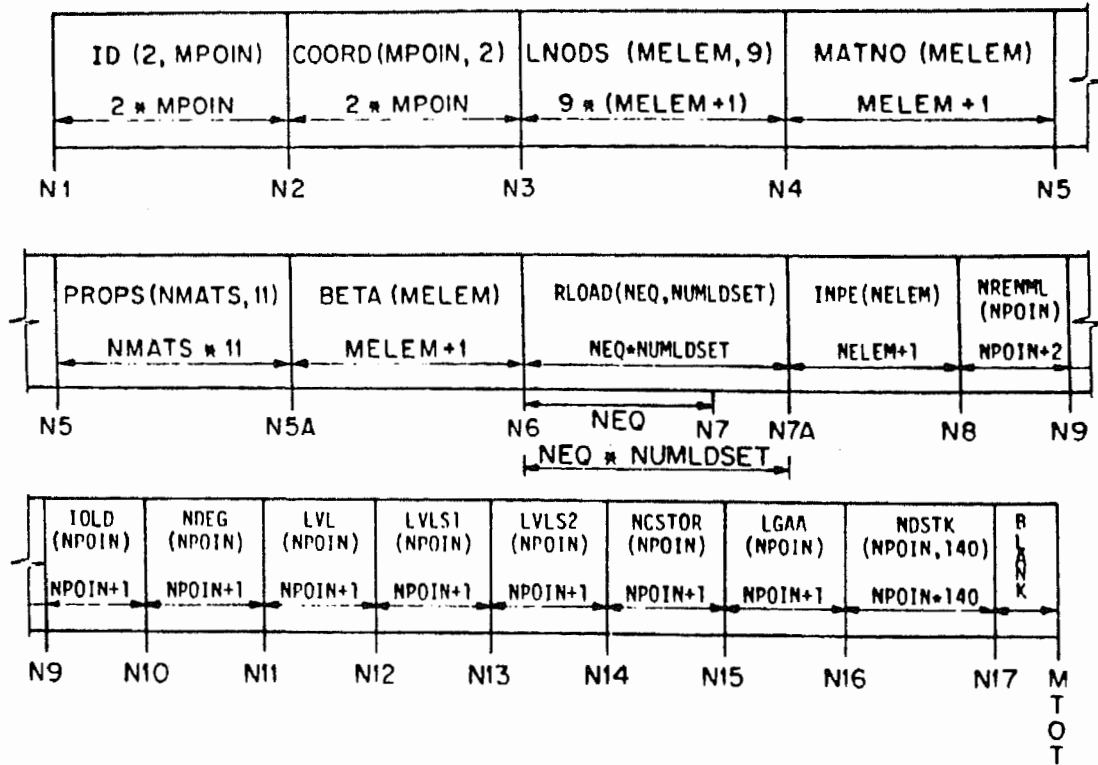


Figure 26a. On Return to MAIN or to CRAPRO from Routine MESHOP.

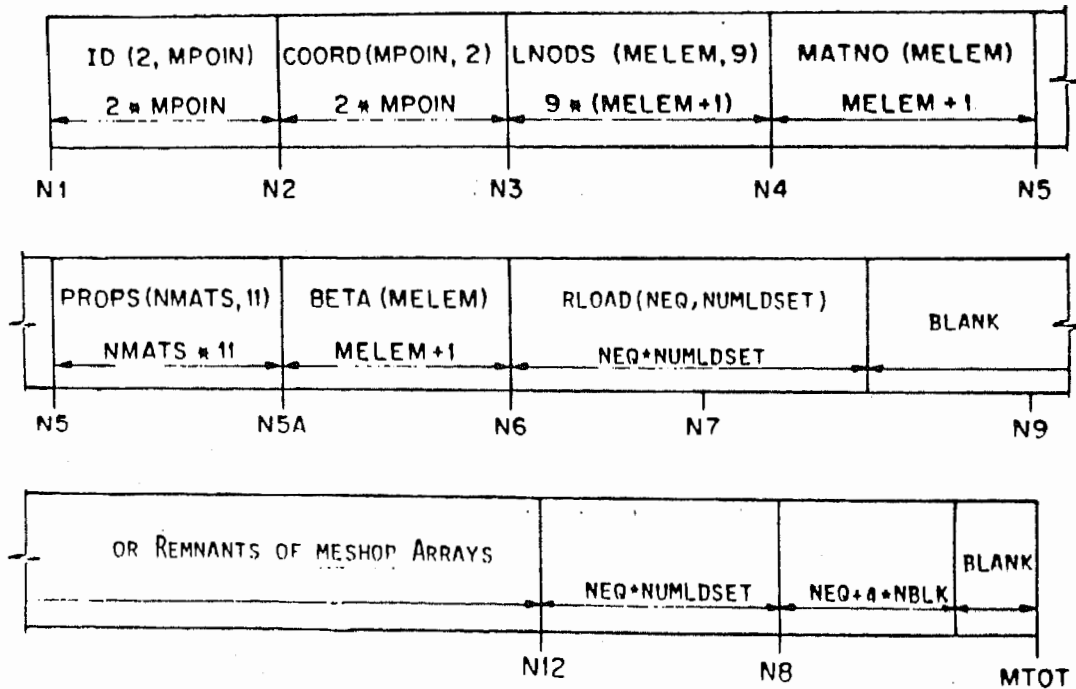


Figure 26b. On Return to MAIN or to CRAPRO from Routine NPOINT(4), Just Prior to Global Stiffness Formation.

Memory Allocation in Principal Storage Vector A

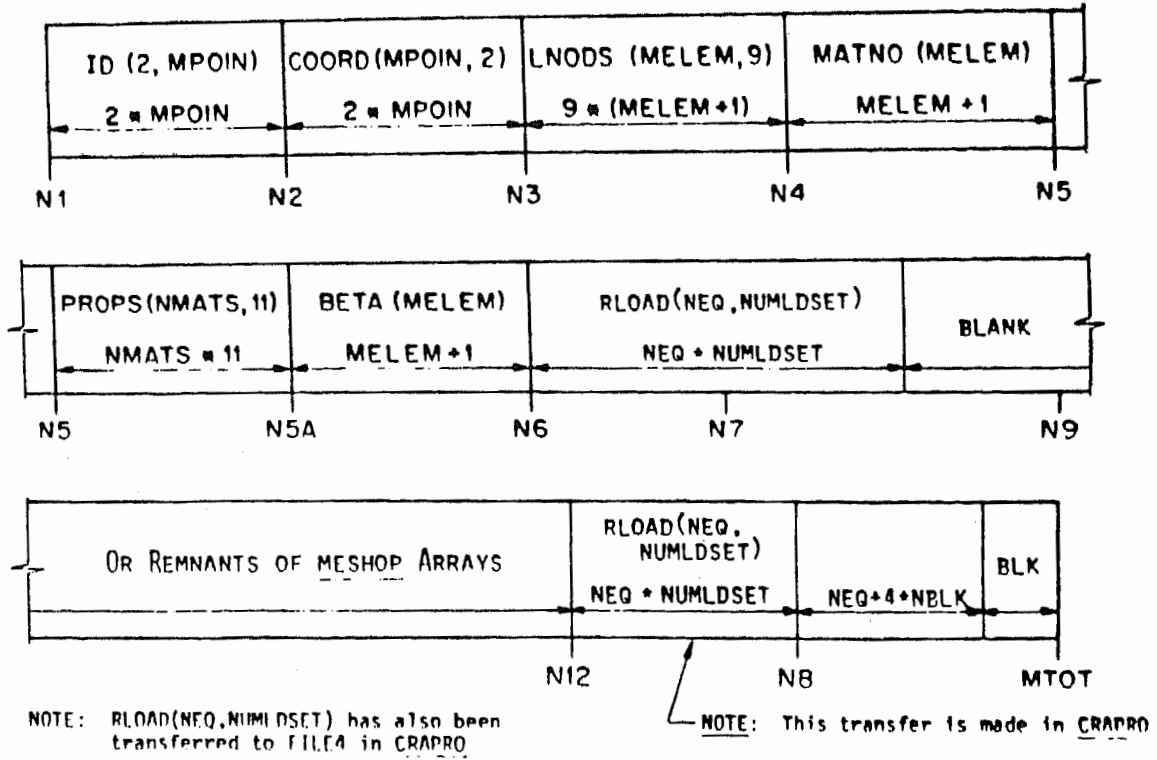


Figure 26c. On First Call to Routine SKY from CRAPRO. Notes: RLOAD has also been written into FILE4 by CRAPRO. The transfer of RLOAD to the N12 location is also made by CRAPRO.

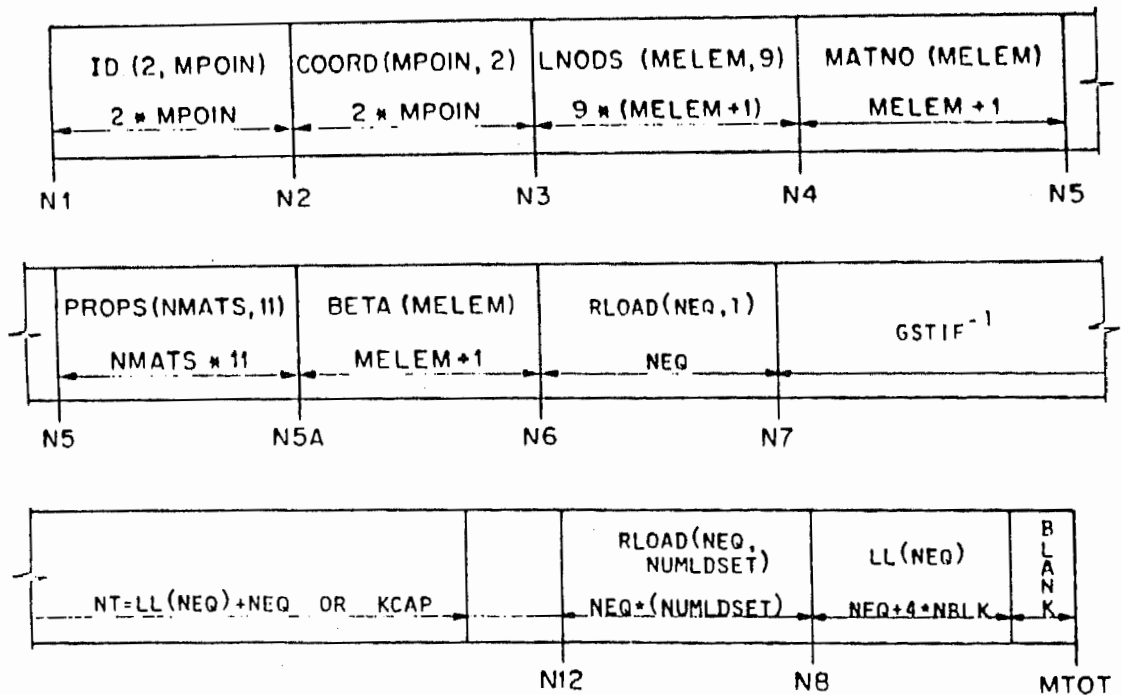


Figure 26d. On First Entry to SKSOLX from SKY for Solution for First Load Set.

Memory Allocation in Principal Storage Vector A

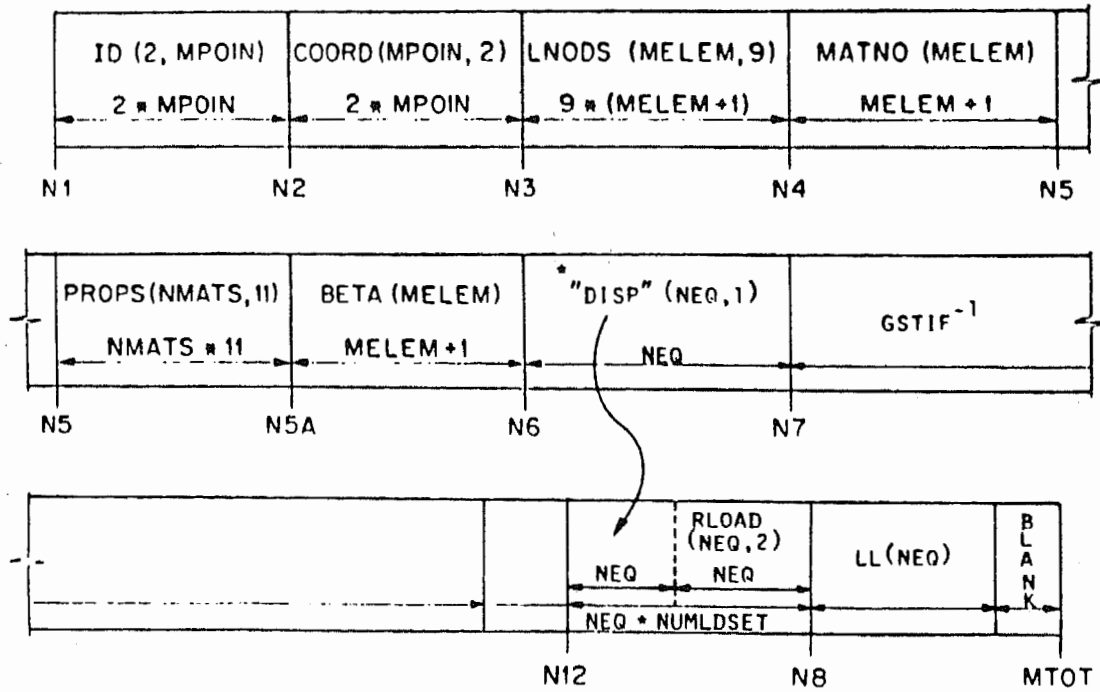


Figure 26e. On Return to SKY from SKSOLX with Solution for First Load Set. Note that "DISP" is not an Actual Variable Name. It is Used Here to Signify that the Approximate RLOAD Vector is Replaced by a Solution Displacement Vector in SKSOLX.

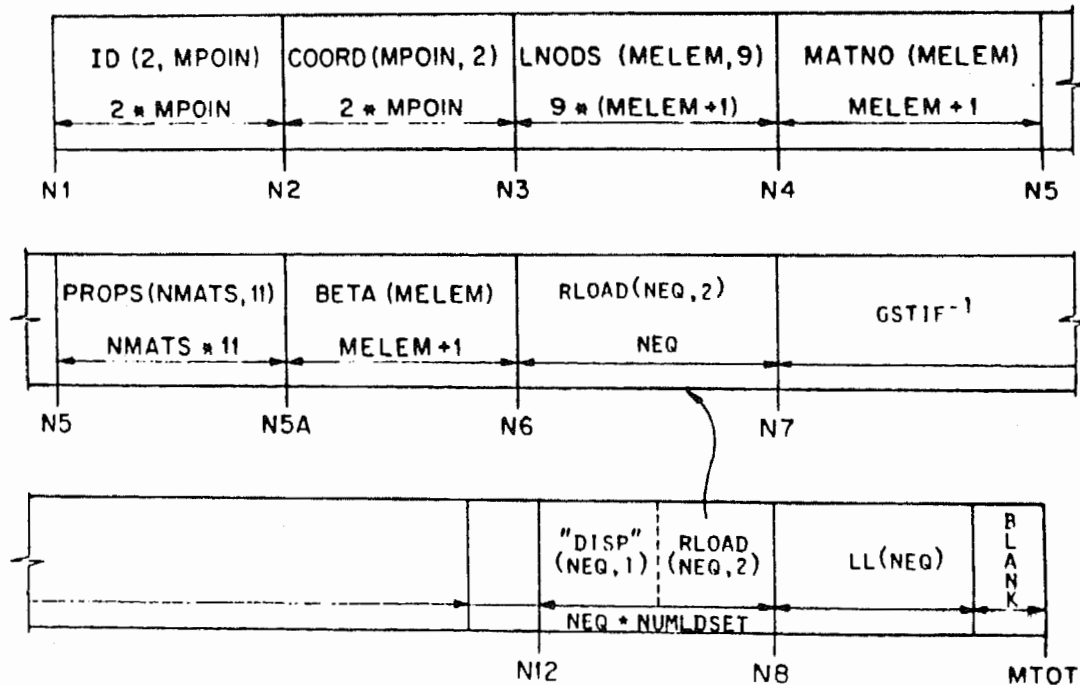


Figure 26f. On Second Entry to SKSOLX from SKY for Solution for Second Load Set.

Memory Allocation in Principal Storage Vector A

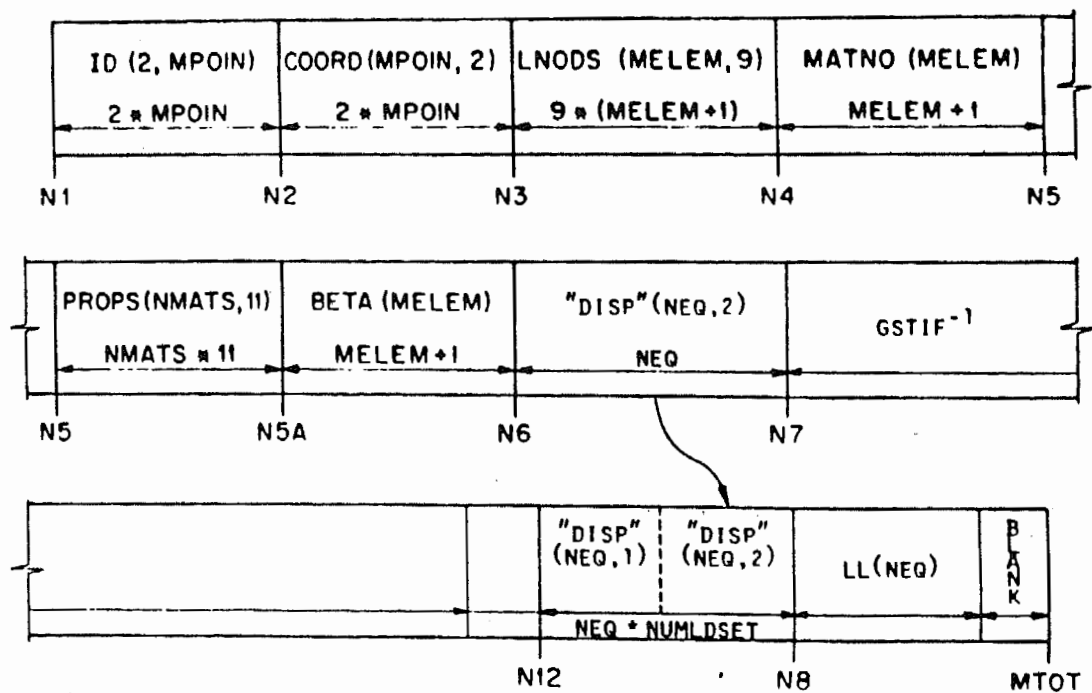


Figure 26g. On Return to SKY from SKSOLX with Solution for Second Load Set.

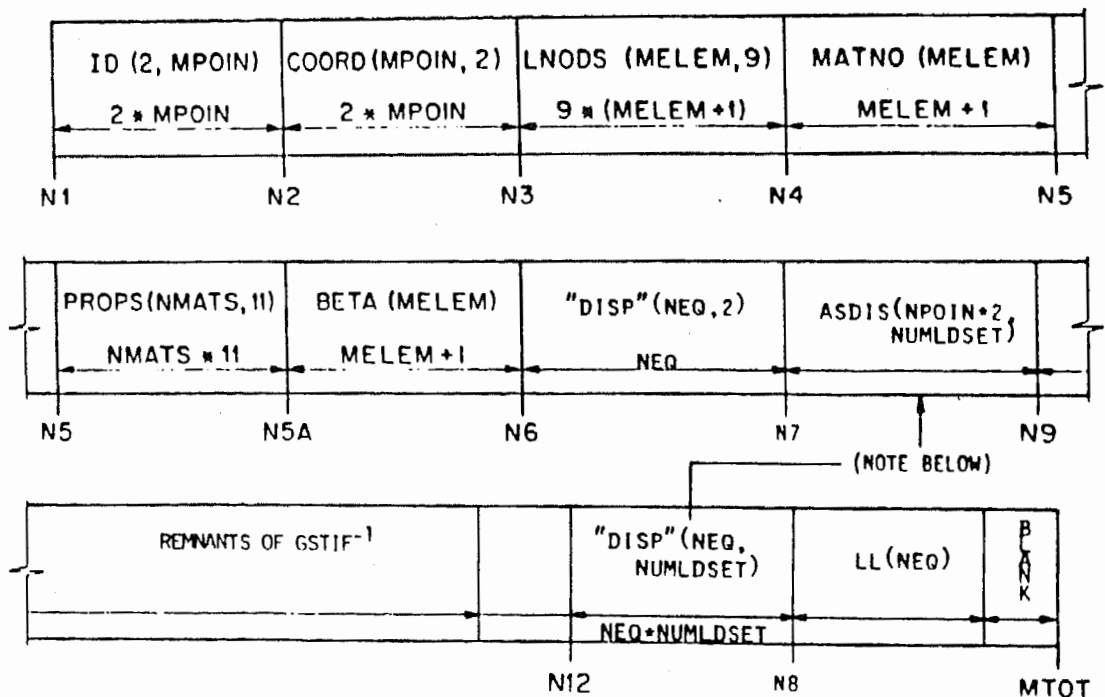
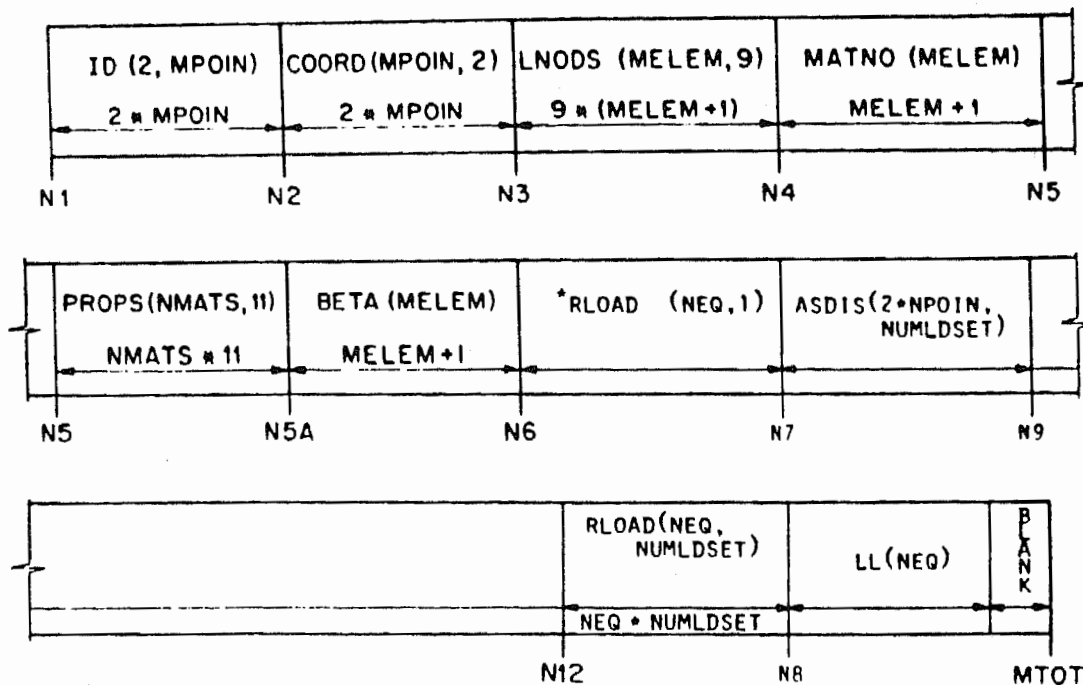


Figure 26h. On Return to SKY from SKYHLP. Note that Restrained and Constrained DOF's are Added to "DISP" to Produce ASDIS.

Memory Allocation in Principal Storage Vector A



* Read from FILE 4

Figure 26i. On Return to CRAPRO from SKY. Note that RLOAD is replaced at N12 by a Read from FILE4 in SKY.

6. REFERENCES

1. Ingraffea, A.R., "Discrete Fracture Propagation in Rock. Laboratory Tests and Finite Element Analysis", Ph.D. Dissertation, Civil Engineering, University of Colorado, Boulder, 1977.
2. Ingraffea, A.R., and Heuze, F.E., "Finite Element Models for Rock Fracture Mechanics", Int. J. for Numerical and Analytical Methods in Geomechanics, vol. 4, pp. 25-43, 1980.
3. Ingraffea, A.R. and Saouma, V., "Numerical Modeling of Discrete Crack Propagation in Reinforced and Plain Concrete", Application of Fracture Mechanics to Concrete Structures, G.C. Sih and A. DiTommaso editors, Martinus Nijhoff Publishers, 1984.
4. Noorishad, J., Witherspoon, P.A., and Brekke, T.L., "A Method for Coupled Stress Flow and Analysis of Fractured Rock Masses", Publ. No. 71-6, Civil Engineering, University of California, Berkeley, March, 1971.
5. Heuze, F.E., "JPLAXD: A Finite Element Program for Static Plane and Axisymmetric Analysis of Structures in Jointed Rock", Lawrence Livermore National Laboratory, UCID-19047, 1981.
6. Heuze, F.E., and Barbour, T.G., "New Models for Rock Joints and Interfaces", ASCE J. Geotech. Eng. Div., vol. 108, no. GT5, pp 757-776, May, 1982.
7. Clough, R. W., "The Stress Distribution of Norfork Dam," Structures and Materials Research, Department of Civil Engineering, Series 100, Issue 19, University of California, Berkeley, March 1962.
8. Ngo, D. and Scordelis, A. C. "Finite Element Analysis of Reinforced Concrete Beams", Journal of the American Concrete Institute, Vol. 64, No. 14, pp. 152-163, March, 1967.
9. Nilson, A. H. "Nonlinear Analysis of Reinforced Concrete by the Finite Element Method", Journal of the American Concrete Institute, Vol. 65, No. 9, pp. 757-776, September, 1968.
10. Mufti, A. A., Mirza, M. S., McCutcheon, J. O., and Houde, J., "A Study of the Behavior of Reinforced Concrete Elements", Structural Concrete Series No. 70-5, McGill University, 1970.
11. Rashid, Y. R., "Analysis of Prestressed Concrete Pressure Vessels", Nuclear Engineering and Design, Vol. 7, No. 4, pp. 334-344, April, 1968.
12. Dodds, R. H., Darwin, D., Smith, J. L., and Leibengood, L. D., "Grid Size Effects with Smeared Cracking in Finite Element Analysis of Reinforced Concrete", Structural Engineering and Engineering Materials SM Report No. 6, The University of Kansas, Lawrence, August, 1982.
13. Mindess, S. and Diamond, S., "The Cracking and Fracture of Mortar", Fracture in Concrete (W. F. Chen and E. C. Ting, eds.), Proceedings of an ASCE Session, Hollywood, Florida, American Society of Civil Engineers, NY, 1980.

14. Ngo, D., "A Network-Topological Approach for the Finite Element Analysis of Progressive Crack Growth in Concrete Members", Ph.D. Dissertation, Division of Structural Engineering and Structural Mechanics, University of California, Berkeley, UC-SESM 75-6, 1975.
15. Haber, R. B., Shephard, M. S., Abel, J. F., Gallagher, R. H. and Greenberg, D. P., "A General Two-Dimensional Graphical Finite Element Processor Utilizing Discrete Transfinite Mappings", International Journal for Numerical Methods in Engineering, Vol 17, No. 7, pp. 1015-1044, July, 1981.
16. Perucchio, R., Ingraffea, A. R., and Abel, J. F., "Interactive Computer Graphic Preprocessing for Three-Dimensional Finite Element Analysis", International Journal for Numerical Methods in Engineering, Vol. 18, No. 6, pp. 909-926, June, 1982.
17. Perucchio, R. and Ingraffea, A. R., "Interactive Computer Graphic Preprocessing for Three-Dimensional Boundary-Integral Element Analysis", Computers and Structures, Vol. 16, No. 1-4, pp.153-166, 1983.
18. Gibbs, N. E., Poole, W. J., and Stockmeyer, P. K., "An Algorithm for Reducing the Bandwidth and Profile of a Sparse Matrix", SIAM Journal of Numerical Analysis, Vol. 13, pp. 236-250, 1976.
19. Catalano, D. and Ingraffea, A. R., "Concrete Fracture: A Linear Elastic Fracture Mechanics Approach", Department of Structural Engineering Report 82-1, School of Civil and Environmental Engineering, Cornell University, Ithaca, NY, 1982.
20. Arrea, M. and Ingraffea, A. R., "Mixed-Mode Crack Propagation in Mortar and Concrete", Department of Structural Engineering Report 81-13, School of Civil and Environmental Engineering, Cornell University, Ithaca, NY, 1981.
21. Gerstle, W., Ingraffea, A. R., and Gergely, P., "The Fracture Mechanics of Bond in Reinforced Concrete", Department of Structural Engineering Report 82-7, School of Civil and Environmental Engineering, Cornell University, Ithaca, NY, 144 pp, June, 1982.
22. Petersson, P-E., "Crack Growth and Development of Fracture Zones in Plain Concrete and Similar Materials", Report TVBM-1006, Division of Building Materials, Lund Institute of Technology, Lund, Sweden, 1981.
23. Gerstle, W., Ingraffea, A. R., and Gergely, P., "Tension Stiffening: A Fracture Mechanics and Interface Element Approach", Proceedings International Conference on Bond in Concrete, Paisley, Scotland, pp. 97-106, June, 1982.
24. Hillerborg, A., Modeér, M., and Petersson, P-E., "Analysis of Crack Formation and Crack Growth in Concrete by Means of Fracture Mechanics and Finite Elements", Cement and Concrete Research, Vol. 6, No. 6, pp. 773-782, 1976.

25. Barsoum, R. S., "On the Use of Isoparametric Finite Elements in Linear Fracture Mechanics", International Journal of Numerical Methods in Engineering, Vol. 10, No. 1, pp. 25-37, 1976.
26. Freese, C. E. and Tracey, D. M., "The Natural Isoparametric Triangle Versus Collapsed Quadrilateral for Elastic Crack Analysis", International Journal of Fracture, Vol. 12, p. 767, 1976.
27. Shih, C. F. de Lorenzi, H. G., and German, M.D., "Crack Extension Modeling with Singular Quadratic Isoparametric Elements", International Journal of Fracture, Vol. 12, pp. 647-651, 1976.
28. Ingraffea, A. R. and Manu, C., "Stress-Intensity Factor Computation in Three Dimensions with Quarter-Point Crack Tip Elements", International Journal of Numerical Methods in Engineering, Vol. 12, No. 6, pp. 235-248, 1978.
29. Erdogan, F. and Sih, G. C., "On the Crack Extension in Plates Under Plane Loading and Transverse Shear", ASME Journal of Basic Engineering, Vol. 85, pp. 519-527, 1963.
30. Sih, G. C., "Some Basic Problems in Fracture Mechanics and New Concepts", Engineering Fracture Mechanics, Vol. 5, p. 365, 1973.
31. Sih, G. C., "Strain-Energy-Density Factor Applied to Mixed Mode Crack Problems", International Journal of Fracture, Vol. 10, p. 305, 1974.
32. Sih G. C. and MacDonald, B., "Fracture Mechanics Applied to Engineering Problems - Strain Energy Density Fracture Criterion", Engineering Fracture Mechanics, Vol. 6, p. 361, 1974.
33. Hussain, M.A., Pu, S.L., and Underwood, J., "Strain Energy Release Rate for a Crack Under Combined Mode I and Mode II", Fracture Analysis, ASTM STP 560, pp. 2-28, 1974.
34. Saouma, V., Ingraffea, A. R., and Catalano, D., "Fracture Toughness of Concrete-- K_{Ic} Revisited", Journal of the Engineering Mechanics Division, OASCE, Vol. 108, No. EM6, pp. 1152-1166, 1982.
35. Beech, J. and Ingraffea, A. R., "Three-Dimensional Finite Element Stress Intensity Factor Calibration of the Short Rod Specimen", International Journal of Fracture, Vol. 18, No. 3, pp. 217-229, 1982.
36. Blandford, G. E., Ingraffea, A. R., and Liggett, J. A., "Automatic Two-Dimensional Quasi-Static and Fatigue Crack Propagation Using the Boundary Element Method", Department of Structural Engineering Report 81-3, School of Civil and Environmental Engineering, Cornell University, Ithaca, NY, 1981.

37. Labuz, J. F., Shah, S. P., and Dowding, C. H., "Post-Peak Tensile Load-Displacement Response and the Fracture Process Zone in Rock", Proc. 24th U.S. Symposium on Rock Mechanics, Texas A&M University, June 20-23, pp. 421-427, 1983.
38. Evans, R. H. and Marathe, M. S., "Microcracking and Stress-Strain Curves for Concrete in Tension", Matériaux et Constructions, Vol. 1, No. 1, pp. 61-64, 1968.
39. Fenwick, R. C. and Paulay, T., "Mechanics of Shear Resistance of Concrete Beams", Journal of the Structural Division, ASCE, Vol. 94, No. ST10, pp. 2325-2350, 1968.
40. Witherspoon, P.A., J.S.Y. Wang, K. Iwai, and J.E. Gale "Validity of Cubic Law for Fluid Flow in a Deformable Fracture", Lawrence Berkeley Laboratory, LBL-9557, 1979.
41. Gale, J.E., "The Effect of Fracture Type (Induced vs. Natural) on the Stress-Fracture Closure-Fracture Permeability Relationships", Proc. 23rd U.S. Symp. on Rock Mechanics, Berkeley, CA (AIME, Littleton, CO), 1982.
42. Landau, L.D., and E.M. Lifshitz, Fluid Mechanics, Vol. 6, Pergamon Press, London, 1959.
43. Shaffer, R.J., R. K. Thorpe, A. R. Ingraffea, and F.E. Heuze "Numerical and Physical Studies of Fluid-Driven Fracture Propagation in Jointed Rock", Proc. 25th Rock Mechanics Symposium, (Soc. Min. Eng., Littleton, CO), pp. 117-126, 1984.
44. Marks' Standard Handbook for Mechanical Engineers, Eighth Edition, McGraw-Hill, pp. 3-37, 1979.

7. ACKNOWLEDGMENTS

This report was prepared by the LLNL Unconventional Gas Program for Morgantown Energy Technology Center, Morgantown, WV, under Contract W-7405-ENG-48, with the U. S. Department of Energy.

The authors are grateful to L. Burrow for her fine typing of the manuscript.